NASA Electronic Parts and Packaging (NEPP) Program

NEPP Task:

Screening Techniques for Ceramic Capacitors with Microcracks

Part II. Leakage and Absorption Currents and Voltages in Ceramic Capacitors

Alexander Teverovsky
Dell Services Federal Government, Inc.
work performed for Code 562, GSFC
Alexander.A.Teverovsky@nasa.gov

2013

Summary

Multilayer ceramic capacitors (MLCCs) constitute the majority of components used in electronic assemblies and most of their failures are related to cracks that are caused either by insufficient process control during manufacturing, by thermal shock associated with soldering or by flex cracking during handling and/or mechanical testing of the circuit boards. These cracks if not identified might cause failures after month and even years of operation and the failure mode varies from a short circuit to intermittent or "noisy" behavior that in some cases might be misjudged as software failures.

To prevent crack-related failures one need a good understanding of the origin of cracks, factors affecting their occurrence, and mechanisms of parametric degradation in fractured capacitors. This is also necessary for a better understanding of possible failure mechanisms in variety of new technology ceramic RF surface mount components. Development of techniques and test methods that would allow revealing defective or potentially weak parts prone to cracking before using them in high-reliability applications also requires in-depth analysis of the degradation processes in capacitors with cracks.

This NEPP task is focused on evaluation of the effectiveness of different existing and new testing techniques for screening and qualification of low-voltage MLCCs that comprise the majority of ceramic capacitors used in space projects. A wide range of commercial and military-grade parts, mostly X7R type, from various vendors with different EIA sizes (from 0402 to 2225), values (from 0.01 μF, to 100 μF) and rated voltages from 6.3 V to 100 V) were used to reveal common features in behavior of normal and fractured capacitors and evaluate test methods.

Several techniques that have been analyzed for this task and preliminary assessments of their effectiveness are shown in Table I below. None of the techniques can be considered as a panacea, but their combination and justified application might assure the necessary level of quality and reliability of the parts.

A NEPP report published in 2011 (Part I of the task) provided insight into mechanisms of electrical breakdowns in capacitors with cracks and evaluated techniques that are based on measurements of breakdown voltages in MLCCs. This year report considers currents in ceramic capacitors, evaluates the significance of insulation resistances (IR), and analyzes the effect of cracking on currents and absorption voltages in low-voltage MLCCs. The next year report will consider long-term degradation of leakage current in fractured capacitors at different voltages, temperatures, and relative humidity of environments. Preliminary data obtained so far indicate the possibility of developing a technique that would distinguished fractured capacitors reliably and in combination with stress testing reveal potentially weak parts. This technique can replace currently used humidity steady state low voltage testing, HSSLV, and will be effective for both, PME and BME types of capacitors.

In this report, it is shown that absorption currents prevail over the leakage currents during standard IR measurements. Absorption currents, and therefore IR, have weak temperature dependence, increase linearly with voltage (before saturation), and most importantly, are not sensitive to the presence of mechanical defects. Intrinsic leakage currents increase superlinearly with voltage and exponentially with temperature (activation energy is in the range from 0.6 eV to 1.1 eV). Leakage currents related to the presence of tiny cracks have a weaker dependence on temperature and voltage, so intrinsic leakage currents are prevailing at high temperatures and voltages thus masking the presence of cracks. For this reason measurements at low temperature and voltages would be more effective for revealing capacitors with cracks. However, leakage currents at low voltages are small, their accurate measurement is

difficult, and the defect-related currents, except for cases with severe fracturing, are typically below the sensitivity level of the electrometers used. It is shown that the time to voltage roll-off and the rate of decrease of absorption voltages with time are related to leakage currents and allow for accurate enough assessments of the insulation resistance at low voltages. Experiments show that measurements of absorption voltages can be used to discriminate normal and fractured capacitors. A simple model that is based on the Dow equivalent circuit for capacitors with absorption has been developed. The model allows for assessment of the effective insulation resistance up to 10^{14} ohm at voltages of a few volts only.

Table I. Assessment of different techniques for revealing low-voltage ceramic capacitors with cracks.

Technique	Effectiveness	Ease of implementation	Comments
Visual examination/vicinal illumination	✓ ✓	✓ ✓	Limited to termination-free areas of the surface.
AC characteristics/ C, DF	-	NA -standard test	not effective
Dielectric Withstanding Voltage, DWV	-	NA -standard test	not effective
Breakdown voltage	✓ ✓	✓ ✓ ✓	Destructive test; can be used for qualification purposes only.
Insulation resistance, IR	-	NA -standard test	not effective
Absorption voltage	✓ ✓	✓ ✓	Requires long-term measurements.
Acoustic microscopy	✓ ✓	✓ ✓	Limited to terminations-free areas; requires skills.
Electromechanical resonance	✓	✓	Reproducibility, effect of prehistory, acceptance criteria?
Methanol test	✓	✓ ✓	Reproducibility, acceptance criteria?
Radiography	✓	NA -standard test	Limited to cases when cracks are aligned with X-rays.
Humidity steady state low voltage test, HSSLV	✓	NA -standard test	Analysis of electrochemical migration in PME and BME capacitors in 2013.
Degradation of leakage currents	✓ ✓	✓ ✓ ✓	Results and analysis in 2013.

Leakage and Absorption Currents and Voltages in Ceramic Capacitors

Contents

Summary 2
I. Introduction 4
II. Experiment 7
III. Time dependence of absorption currents 10
IV. Effect of voltage on absorption and leakage currents 14
V. Effect of temperature on absorption and leakage currents 18
VI. Effect of cracking on absorption and leakage currents 25
VII. Absorption capacitance 29
VIII. Modeling of absorption currents 33
IX. Modeling of absorption voltages 35
X. Absorption voltages in virgin and fractured capacitors 40
XI. Discussion 47
- Absorption currents 48
- Intrinsic leakage currents. 51
- Leakage currents caused by mechanical defects. 56
- IR measurements based on absorption voltages. 56

XII. Conclusion 57
XIII. References 58

I. Introduction

If an ideal capacitor C_0 is charged from a power supply V_0 through a resistor R_0, the charging current $i(t)$ will decrease and voltage across the part $u(t)$ will increase exponentially with time:

$$i(t) = \frac{V_0}{R_0} \times \exp\left(-\frac{t}{\tau_0}\right) \qquad (1.1)$$

$$u(t) = V_0\left[1 - \exp\left(-\frac{t}{\tau_0}\right)\right],$$

where $\tau_0 = R_0 \times C_0$ is the characteristic time of the charging process. At $t > 3 \times \tau_0$ the current will be negligibly small (below 5% of the initial value) and the voltage across the part will stabilize at V_0. Short circuiting of the capacitor for a period ~ $3 \times \tau_0$, will discharge the part almost completely and the voltage will remain close to zero at any moment of the storage time. Note that even at relatively large R_0 and C_0 values, when R_0 is in the kiloohm range and C_0 is in the microfarads range, τ_0 is in the milliseconds range, so the charging and discharging processes are completed within a second, and does not affect measurements of DC currents in capacitors within one or two minutes after voltage application that are required to determine the value of the insulation resistance, IR.

Real capacitors behave differently. After a charging period ~$3\tau_0$, the current continue decreasing with time relatively slowly and when such a capacitor is left disconnected after a brief short circuit period, the voltage across the electrodes will increase with time. This behavior is due to polarization processes in the dielectric that might include dipole orientation, redistribution of ionic charges, charge injection from electrodes, or electron tunneling into the traps in the dielectric [1]. We are considering here relatively slow polarization processes, so fast processes similar to electronic polarization and domain wall polarization [2] are excluded. Disregarding the specific physical mechanism of polarization, a slow (from seconds to hours) decrease of currents with time after application of a voltage step can be described as a process of charge absorption. Increasing of voltage after a brief short circuit of a capacitor is also due to absorbed charges that are released back to the electrodes. Currents and voltages related to these processes are defined as absorption currents and absorption voltages. The first includes polarization currents under poling conditions and depolarization currents under short circuit conditions, and the latter in technical literature is often referred to as dielectric absorption (DA).

Absorption processes are well known in variety of dielectric materials employed in different types of capacitors including polymer capacitors [3-7], tantalum capacitors [8-10], and ceramic capacitors [11-13]. Absorption currents in these capacitors typically follow the empirical Curie von Schweidler law that in some publications this is referred to as a Kohlrausch behavior [14-15]. According to this law, polarization currents decrease with time as a power function:

$$I(t) = I_0 \times t^{-n} \ , \qquad (1.2)$$

where I_0 and n are constants, and n is close to 1.

Absorption voltage in capacitors can limit the accuracy and cause errors in analog applications employing sample-and-hold circuits, integrating analog-to-digital converters and active filters [4]. DA is also a source of errors in the voltage-to-frequency transfer circuits of voltage controlled oscillators, VCO [16]. In earth sensors for satellites a charge transferred to a capacitor can create spurious signals [17]. To reduce the effect of DA in sensitive applications designing of special compensating circuits might be necessary [18].

MIL-PRF-19978 specifies measurements of DA: a capacitor shall be charged at the DC voltage rating for 1 hour, discharged for 10 seconds, and the recovery voltage shall be measured with a voltmeter having an input resistance of 10,000 Mohm or greater at the maximum voltage within a 15 minute period. The dielectric absorption shall be calculated as a ratio of the maximum recovery voltage to the charging voltage. Literature data indicate that DA is larger for high-k ceramic materials and decreases

substantially for polypropylene and Teflon capacitors [4]. Polyphenylene sulfide (PPS) dielectric capacitors have DA ~ 0.02% to 0.05%, ceramic COG capacitors ~0.5%, and X7R - Z5U capacitors up to 1 – 1.8% [11].

Absorption voltage depends on the polarization conditions (applied voltage and time of polarization), discharge time, and time of recovery. All these conditions vary substantially for different applications, and most circuit designers are concerned about short-term effects of DA [16]. For this reason, the specified method of DA measurements has a limited value and to some degree can be used only to assess a relative capability of different materials for voltage recovery. Most literature data related to DA were obtained within seconds or minutes after shorting, and there is no information on the long-term behavior of absorption voltage in capacitors. This behavior is important to understand possible degradation of capacitors during storage, and also, as it will be shown in this report, it might provide useful information about the presence of mechanical defects in MLCCs.

Insulation resistance (IR) in MLCCs is considered an important parameter that assures that no significant defects in the dielectric are present. Cracks in ceramic capacitors are assumed to increase leakage currents and reduce IR, so during screening and qualification processes parts with IR below the specified limit are considered normal and free of structural defects.

At +25°C military specifications require IR to be greater than 100,000 megohms or 1,000 megohm-microfarads, whichever is less and at +125°C 10,000 megohms or 1000 megohm-microfarads, whichever is less. High volumetric efficiency commercial MLCCs have somewhat relaxed requirements, for example, Murata requires minimum IR = 500 Ohm-F for capacitors greater than 0.047 μF. According to military specifications, IR is determined as a ratio of current measured within 1 or 2 minutes of electrification to the applied rated voltage. The same test conditions are typically used for commercial capacitors; however, mass production requires high-speed testing techniques, and manufactures are looking for test systems that would allow IR measurements at much shorter periods of time, within seconds [19].

Understanding of absorption and leakage currents in normal and fractured ceramic capacitors, in particular the effect of voltage and temperature, is essential for assessment of the effectiveness of existing screening procedures to select high quality capacitors for space applications. This is especially important for new, high value MLCCs where absorption currents might prevail over the leakage currents and determine the value of insulation resistance of the part. In this case the significance of IR for quality control purposes might be reduced substantially.

The purpose of this work is to get insight into absorption and leakage currents in low-voltage MLCCs, investigate voltage and temperature dependencies of these currents, and assess their sensitivity to the presence of cracks. A comparative analysis of long-term (up to several hundreds of hours) variations of absorption voltages for normal capacitors and capacitors with cracks has been carried out to assess the voltage absorption measurements for revealing capacitors with cracks and get more information about possible degradation processes in MLCCs during storage.

II. Experiment

A variety of MLCCs produced by seven different vendors were used in this study to reveal common features in absorption currents and voltages. Most of the parts were commercial, base metal electrode, BME, (nickel) high volumetric efficiency X7R capacitors. Some parts were manufactured per military specifications using silver-palladium metallization, so-called precious metal electrodes, PME, capacitors. The size of the capacitors varied from 0402 to 2225, rated voltage from 6.3 V to 100 V and capacitance from 1500 pF to 100 μF.

Leakage currents were measured using a PC-based data acquisition system that allowed for monitoring currents by measuring voltage drop across a resistor connected in series with each capacitor (typically 100 kOhm). Currents below 1 nA and absorption voltages were measured using different Agilent source-measuring units (SMU) that allow voltage measurements with the effective internal resistance of better than 10^{13} ohm.

To evaluate the effectiveness of different testing techniques, groups of virgin capacitors and capacitors with cracks with sizes from 3 to 20 pcs. have been tested. One of the challenges of this task is introducing cracks in the part. The technique used for crack generation should mimic real life conditions and only cracks penetrating into active area of capacitors are of interest. In this study, the defects were introduced using three techniques that have different benefits and drawbacks:

1. Mechanical fracture. In some cases a corner portion of the part was chipped-off using fine cutters, in others a part was scratched using a diamond scriber and cleaved along the scratch.
2. Local fracturing. A capacitor was damaged by a hit with a Vickers indentor of by applying pressure to the surface of the capacitor with a tungsten carbide scriber 88CM-type tool (General Tools).
3. Thermal shock. Capacitors were stresses by a cold thermal shock using the ice water testing (IWT) technique described in [20] or hot thermal shock using a solder dip test.

Figures 2.1 to 2.3 below show examples of capacitors with cracks formed using different techniques.

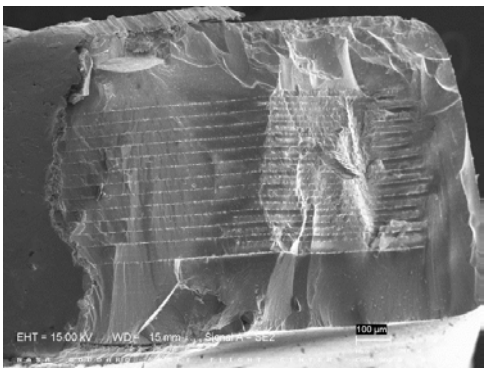

Figure 4.1. Example of a chip-out in a 2220 Mfr.C 1 μF 50 V capacitor.

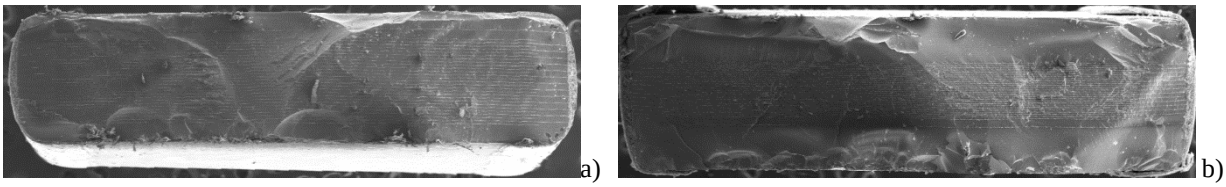

Figure 4.2. Scribed and cleaved 1825 PME 0.47 μF 50 V (a) and BME 1 μF 50 V (b) capacitors from manufacturer C.

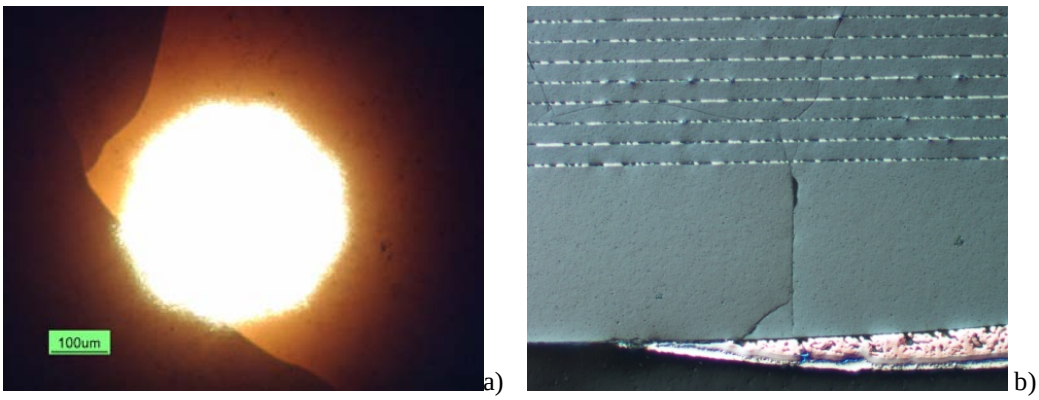

Figure 4.3. Vicinal illumination (a) and cross-sectional (b) views of a Mfr.A 1 μF 50 V capacitor showing cracks after ice water test thermal shock at 250 °C, IWT_250.

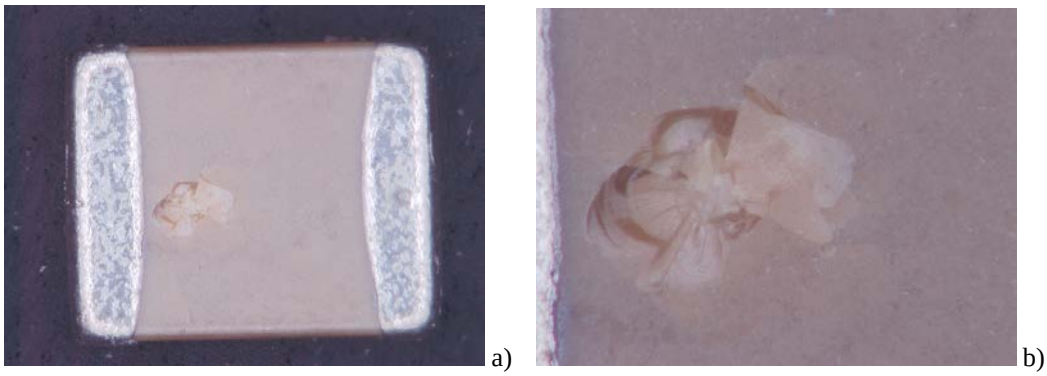

Figure 4.4. Overall (a) and close-up (b) views of damage caused by Vickers indenter in a 1210 Mfr.A 0.1 μF 50 V X7R capacitor.

These techniques were used to simulate manufacturing or assembly/handling related cracking in ceramic capacitors and have different advantages and drawbacks in approaching this goal. Mechanical fracturing guarantees that internal electrodes are exposed to environments, but the processes on the cleaved surface might be somewhat different compared to the processes in cracks (water surface adsorption compared to water capillary condensation). Ice water testing forms cracks that are filled with water initially, and baking the capacitors to simulate "dry" conditions might be not sufficient. Solder dip testing might create surface cracks that do not affect active areas of the capacitors. Indenter or

tungsten carbide tool caused local damage that might provide the closest simulation to the real life cracking, but there is no guarantee that the crack penetrates deep enough to cross internal electrodes.

AC characteristics of the parts (capacitance, C, and dissipation factor, DF) were measured using Agilent 4294 precision impedance analyzer at 1 kHz. Only parts with acceptable AC characteristics were used for the following tests. In most cases fracturing did not cause significant variations of C and/or DF (see Figure 4.5). This suggests that AC characteristics are not sensitive to the presence of cracks.

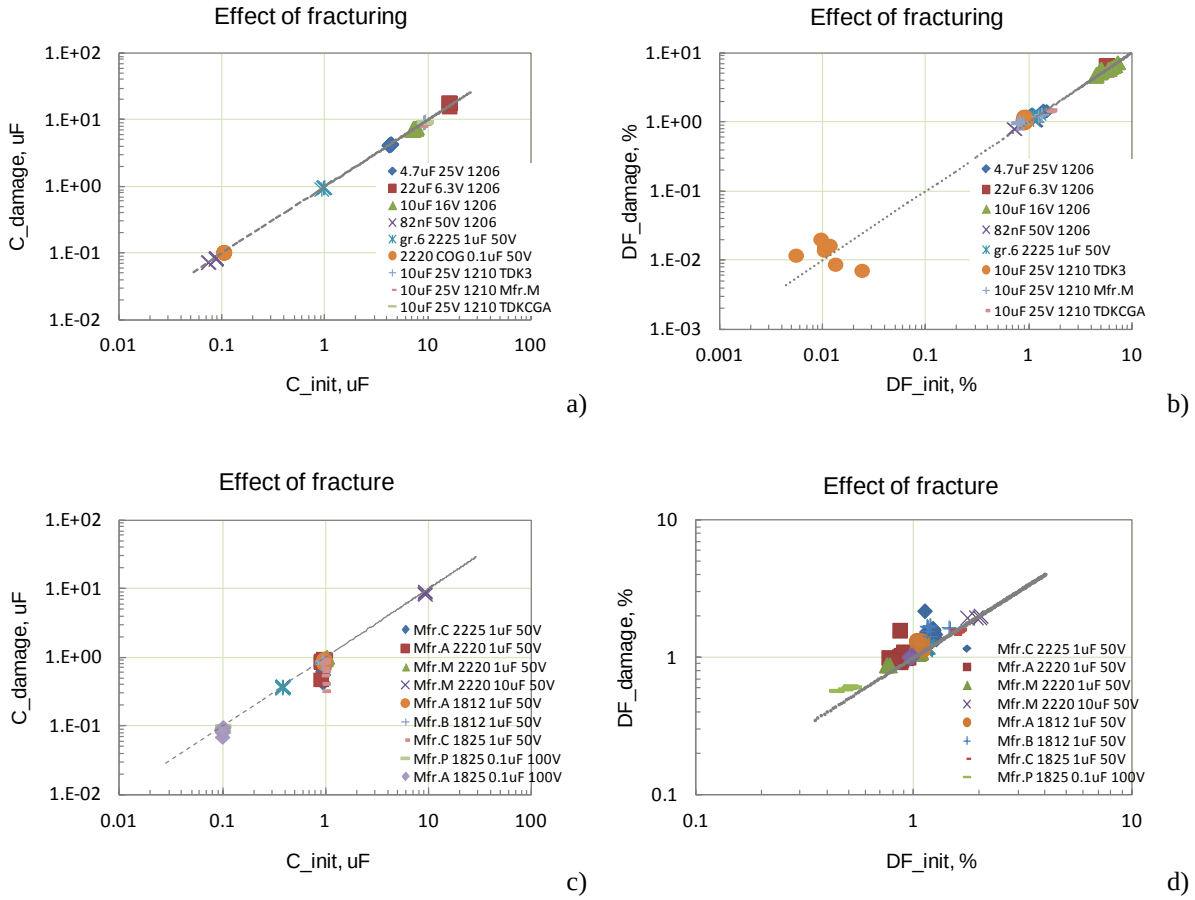

Figure 4.5. Effect of fracturing on capacitance (a, c) and dissipation factors (b, d) of small size (a, b) and large size (c, d) ceramic capacitors.

In all cases of fractured capacitors considered in this work the presence of cracks in the active area (cracks crossing opposite electrodes inside the part) has been confirmed by measurements of long-term degradation of leakage currents. This technique and results of investigations will be discussed in the next year NEPP report. As an example of long-term degradation of leakage currents Figure 4.6 shows variations of currents with time for 19 fractured and one reference 4.7 µF 25 V capacitors at rated voltage and room conditions (22 °C and 50% RH) for 240 hours. Up to ~ 10 hours currents remain low and decrease with time due to dominance of absorption currents. However, all fractured capacitors had currents increasing with time after dozens of hours of testing.

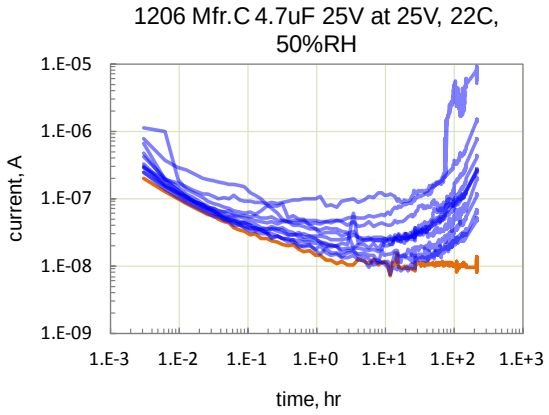

Figure 4.6. An example of long-term degradation of leakage currents in 1206 4.7 μF 25 V capacitors with cracks (blue lines) and in a normal capacitor (beige line). Note, that per IR requirements the currents after 120 sec (0.033 hr) should be below 1.2×10^{-7} A, so 18 out of 19 parts with cracks would be considered acceptable.

III. Time dependence of absorption currents

Relaxations of currents in various ceramic capacitors after application of rated voltages are shown in Figures 3.1 to 3.3. In double logarithmic coordinates *I-t* characteristics can be approximated with straight lines over a large period of time, typically from seconds to several hours. This confirms the applicability of the power law, Eq.(1.2), for a long-term current relaxation. Results show that absorption currents are highly reproducible and measurements on groups up to 20 samples showed that all parts have the same amplitudes and the rate of decay. Depending on the part type, the exponent *n* in Eq.(1.2) varied in the range from 0.6 to 1.3.

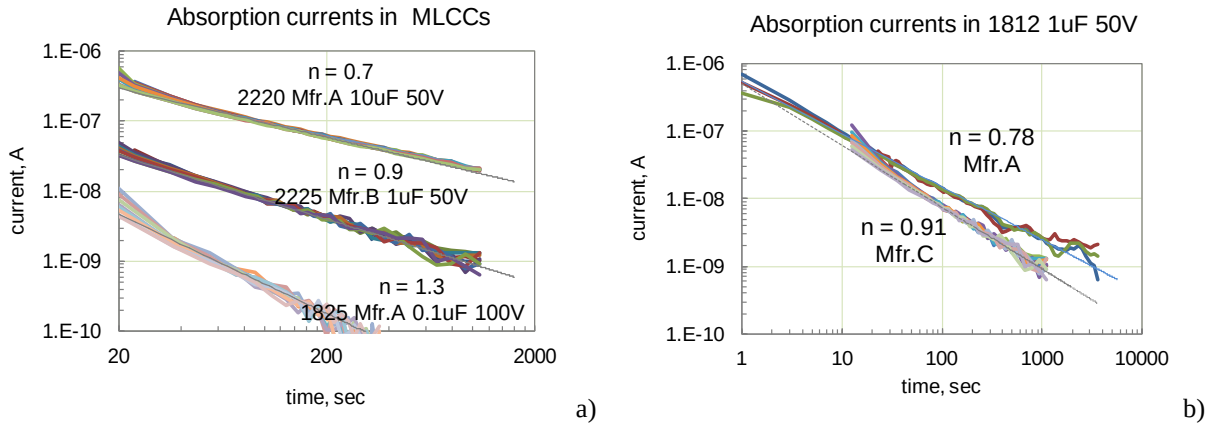

Figure 3.1. Reproducibility of absorption currents in different types of X7R ceramic capacitors. Each group of capacitors has from 3 to 20 samples.

Figure 3.2 shows current relaxation in ceramic capacitors with different types of dielectric, X7R, X5R, and NPO/COG. In all cases the Curie - van Schwendler behavior was confirmed. The level of absorption currents typically increases with capacitance but is similar for COG and X7R types of capacitors. In some cases (see Figure 3.2, 0805 Mfr.R 22 nF 50V and Figure 3.3, 0805 Mfr.C 1mF 6.3V

capacitors) the currents level off after ~ 2000 seconds due to absorption currents decreasing below the intrinsic leakage currents in the parts. Parts with the same size and same value of capacitance might have substantially different (up to order of magnitude) isochronic absorption currents.

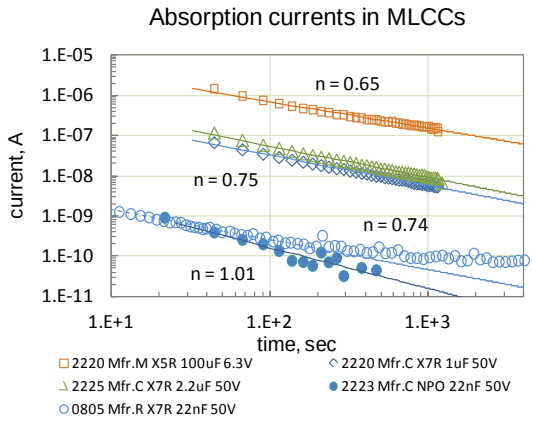

Figure 3.2. Absorption currents in MLCCs with different types of dielectrics (X7R, X5R, NPO).

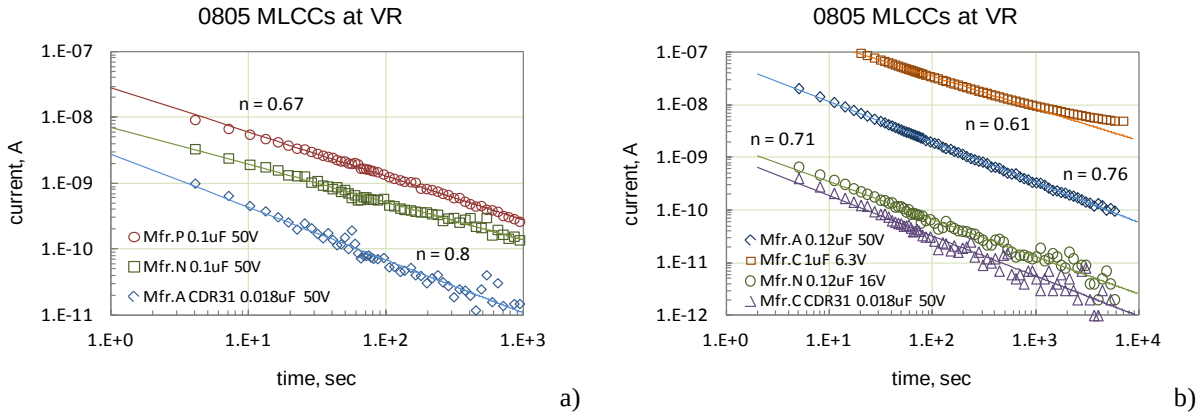

Figure 3.3. Absorption currents in eight types of MLCCs from four different vendors. Note that all capacitors had the same size, 0805.

Figures 3.4 to 3.6 show comparison between polarization and depolarization absorption currents. In all cases the currents were very similar, and although had different polarity, both demonstrate Curie van Schwendler behavior with similar exponents and similar levels of isochronic currents.

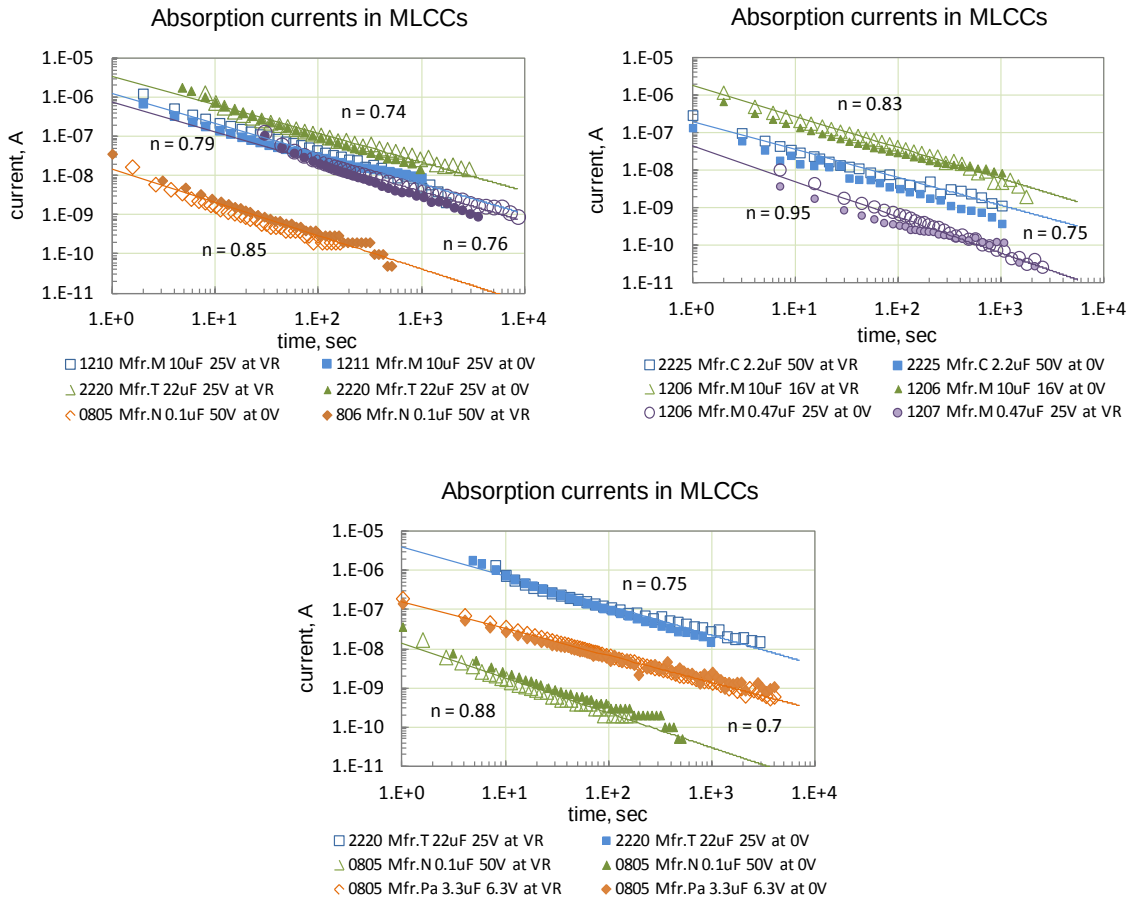

Figure 3.4. Comparison of polarization currents measured at rated voltages (empty marks) and depolarization currents (solid marks) in different types of MLCCs having values in the range from 0.1 μF to 22 μF.

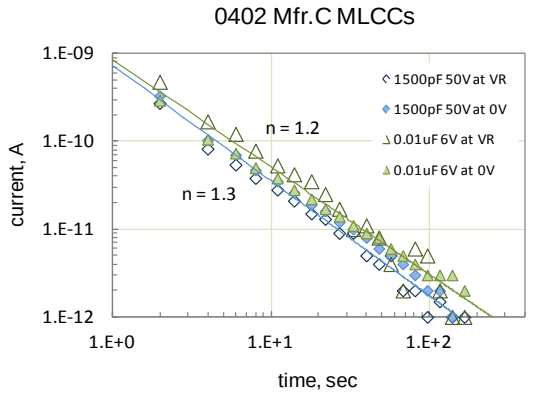

Figure 3.5. Absorption currents in 0402 capacitors at rated voltages (empty marks) and at 0 V (solid marks).

Absorption currents depend strongly on the prehistory of the capacitor. In data shown in Figure 3.6 capacitors were tested for 10 hours with incrementally increasing voltages from 50 V to 100 V with 25V increments. Prior to 100 V testing the parts were not depolarized and for this reason polarization currents at 100 V were much lower and had a different relaxation rate compared to depolarization currents measured after 100 V polarization.

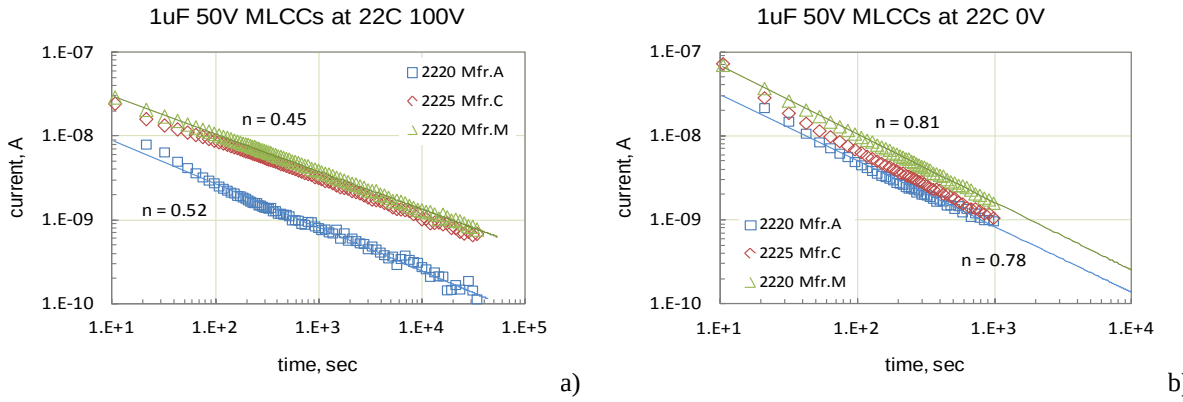

Figure 3.6. Polarization (a) and depolarization (b) currents in 1 μF 50 V capacitors from different vendors. Note that depolarization currents differ compared to polarization currents because polarization at 100 V followed measurements at 75V without depolarization.

Figure 3.7 shows distribution of currents measured in three groups of 1 μF 50 V capacitors produced by the same manufacturer but in different case sizes (EIA codes 2220, 1210, and 0805). These parts were manufactured using the same material, but different thickness of the dielectric: 19.4 μm for 2220, 8.9 μm for 1206, and 4.3 μm for 0805 capacitors. The currents were measured after 60 seconds (time that is typically used for IR measurements) and 1000 seconds of polarization. No substantial difference was observed for 60-sec measurements where absorption currents prevail. However, 1000-sec measurements were almost an order of magnitude less for 2220 parts compared to 0805 capacitors. The results can be explained considering that currents measured after 1000 sec have a substantial component related to the intrinsic leakage currents in the parts, whereas absorption currents are prevailing for 60-sec measurements. Obviously, leakage currents have a strong dependence on the thickness of the dielectric, whereas the absorption currents depend mostly on the value of capacitance.

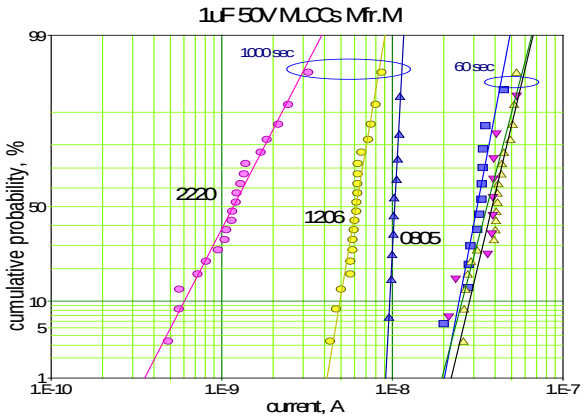

Figure 3.7. Distributions of leakage currents in 1 μF 50V capacitors measured after 60 sec and 1000 seconds of electrification. All parts were from the same manufacturer, but had different case sizes. The thickness of the dielectric was 19.4 μm, 8.9 μm, and 4.3 μm for EIA case sizes 2220, 1206, and 0805 respectively.

IV. Effect of voltage on absorption and leakage currents

An increase in applied voltage increases isochronic absorption currents whereas the rate of current decay that can be characterized by the exponent *n* remains practically the same (see Figure 4.1). At voltages exceeding the rated in 2 to 3 times the current decay levels-off after 100 to 1000 sec due to increased leakage currents. Absorption currents that were measured after 120 sec of polarization are plotted against voltage in Figure 4.2 and indicate a linear dependence of I_{120} on voltage. This formally allows using resistance as a measure of absorption currents in MLCCs; however, this resistance does not reflect the level of intrinsic leakage currents.

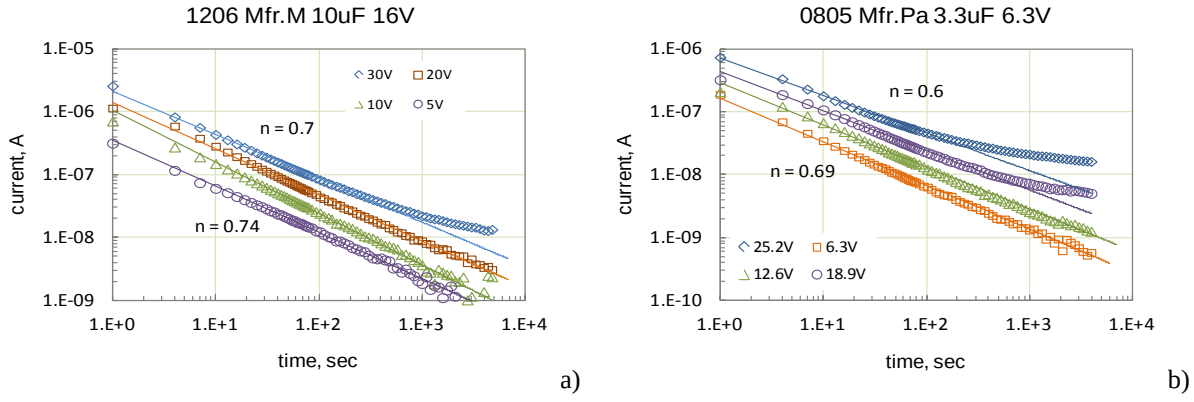

Figure 4.1. Absorptiopn currents at different voltages in 10 µF 16 V (a) and 3.6 µF 6.3 V (b) X7R capacitors.

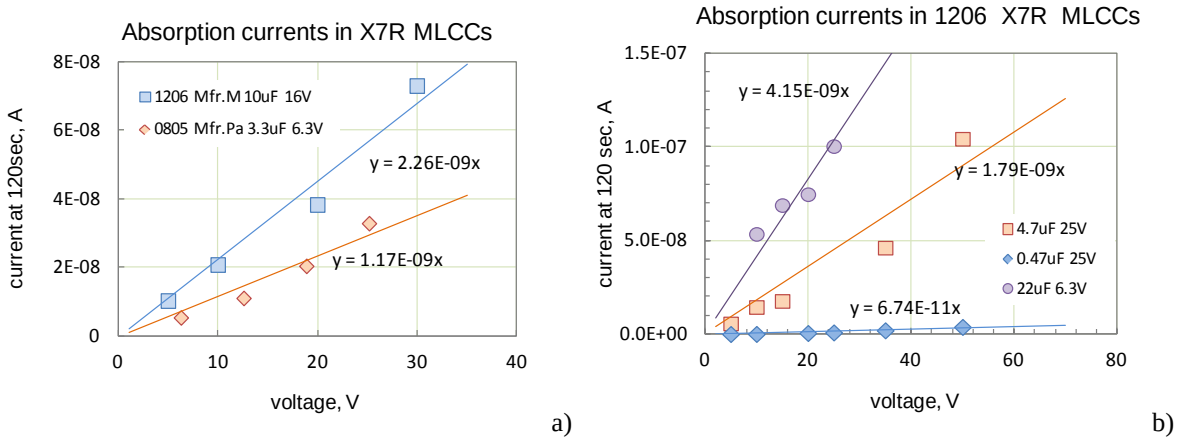

Figure 4.2. Voltage dependence of isochronic currents measured after 120 sec of polarization in five different types of X7R capacitors (see legends).

Figure 4.3 shows that similar to X7R capacitors, NPO capacitors also increase absorption currents with applied voltage linearly.

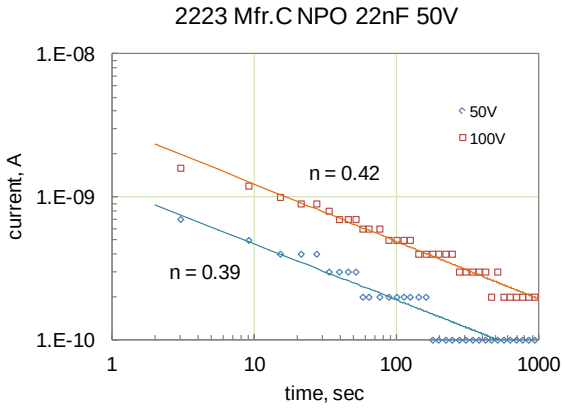

Figure 4.3. Effect of voltage on absorption currents in 22 nF 50 V NPO capacitors.

Figures 4.4 and 4.5 show that when leakage currents increase with voltage substantially and exceed absorption currents by orders of magnitude, depolarization currents remain at the same level and the exponent *n* does not vary significantly. This indicates that the charge absorption processes are independent on the processes controlling leakage currents in ceramic capacitors.

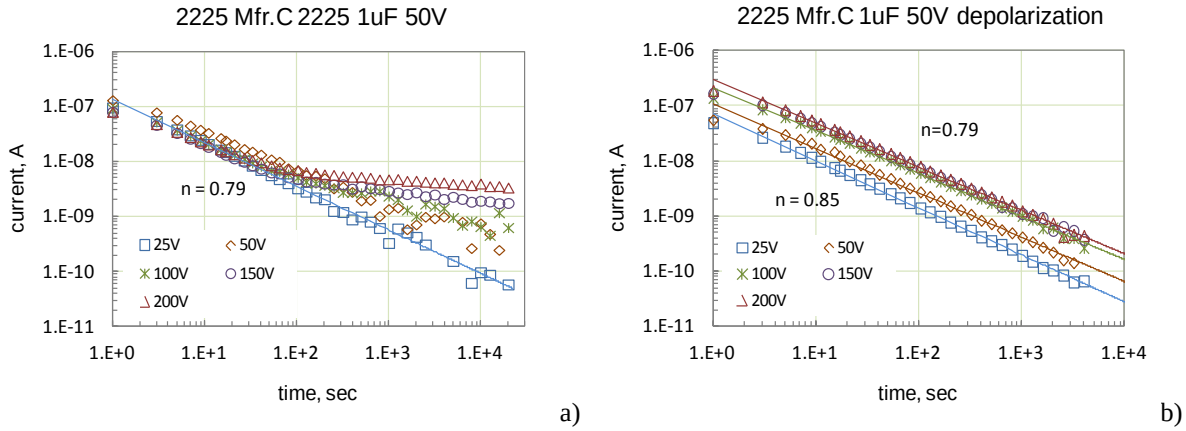

Figure 4.4. I-t characteristics in 1 μF 50V capacitors at different voltages. Figure a) shows polarization and figure b) depolarization currents.

Variations of absorption and leakage currents with voltage for a 3.3 μF 6.3 V capacitor are shown in Figure 4.5 (from c to f). The absorption (depolarization) currents increase linearly up to ~ 25 V and then saturate with voltage. Leakage currents are plotted in Schottky [*ln(I) vs.* $V^{0.5}$], Poole-Frenkel [*ln(I/V) vs.* $V^{0.5}$], and double logarithmic coordinates. Linearization of data in the latter case indicates that the current increases with voltage according to a power law, $I(t) \sim V^m$, where the exponent *m* is a constant. In the two first cases, the linearization suggests respectively either Schottky or Poole-Frenkel mechanisms of conduction. Clearly, in all three cases the data can be linearized equally well, with the correlation factor, R^2, exceeding 0.99. Unfortunately, this does not allow discriminating physical processes responsible for conduction in ceramic capacitors.

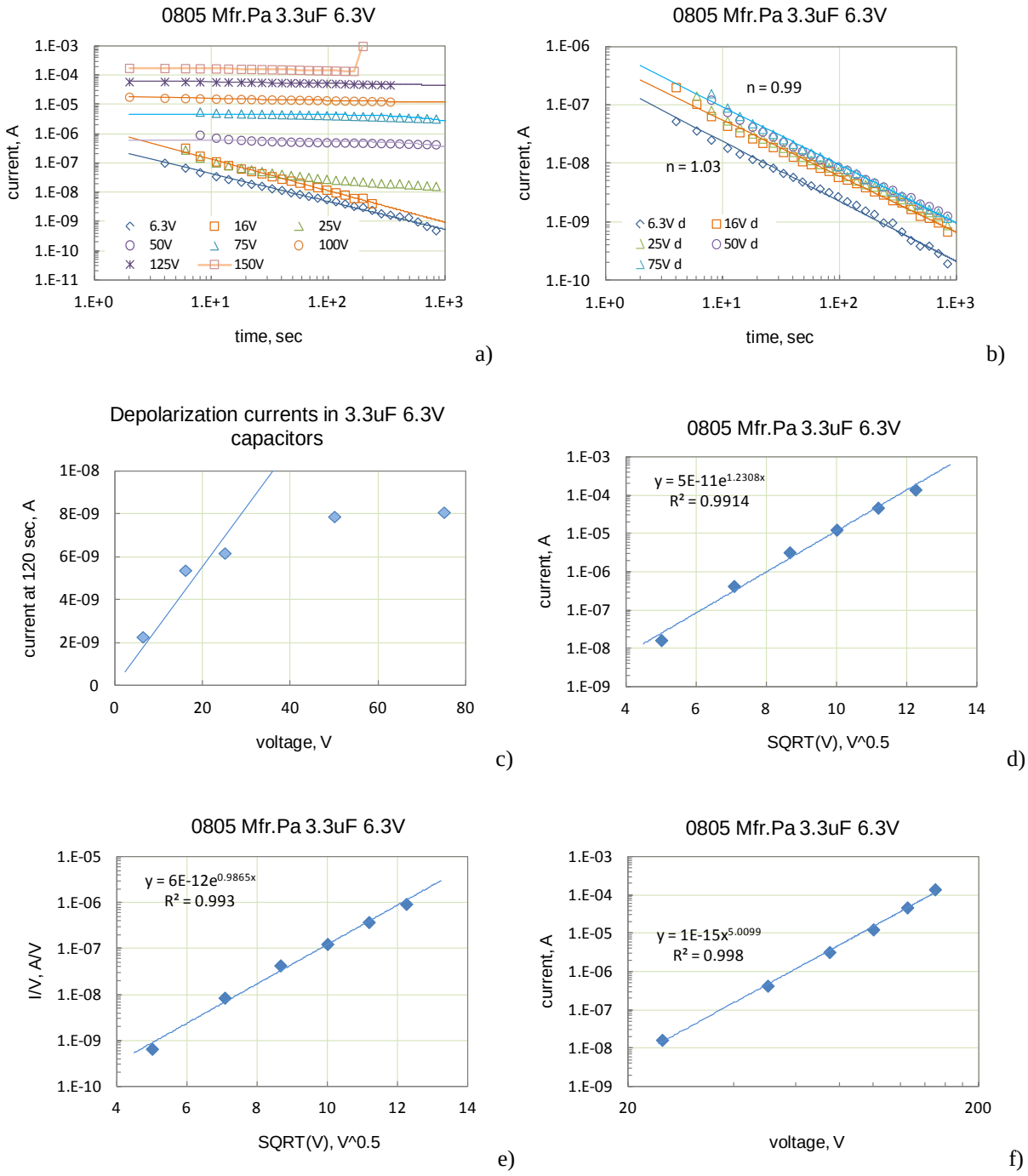

Figure 4.5. Time dependence of polarization (a) and depolarization currents in 3.3 µF 6.3 V capacitors at different voltages. Figure (c) shows variations of depolarization currents measured at 120 sec with voltage. Figures (d), (e), and (f) show I-V characteristics of leakage currents in Schottky (d), Poole-Frenkel (e), and double logarithmic coordinated (f).

Figure 4.6 shows *I-t* and *I-V* characteristics measured for 22 µF 6.3 V X7R capacitors in 1206 cases. Similar to absorption currents, leakage currents are also highly reproducible and remain practically the same from sample to sample. For these parts leakage currents are clearly observed after ~1000 sec of polarization starting from 1.5VR. Similar to the previous case, absorption currents first increase linearly with voltage, and then stabilize. I-V characteristics of leakage currents can be described by exponential

and power laws equally well. The exponent in the power law $m = 2$, which might indicate a space-charge limiting mechanism of conduction.

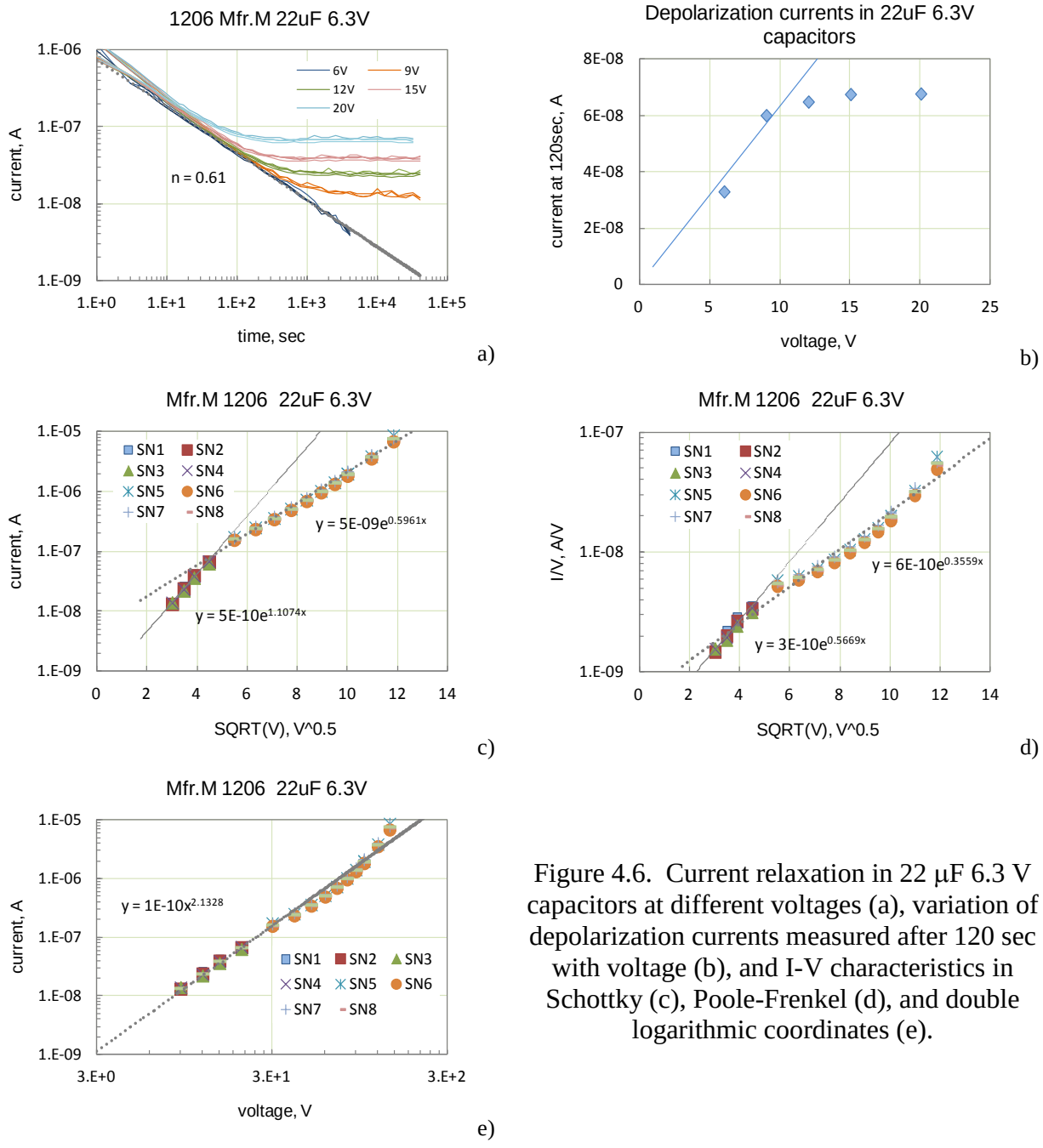

Figure 4.6. Current relaxation in 22 µF 6.3 V capacitors at different voltages (a), variation of depolarization currents measured after 120 sec with voltage (b), and I-V characteristics in Schottky (c), Poole-Frenkel (d), and double logarithmic coordinates (e).

Relaxation of currents at voltages in the range from 6 V to 100 V and the relevant I-V characteristics for L2L 0.68 µF 6.3V capacitors used in V4 XILINX FPGAs are shown in Figure 4.7. The part has a size 0508 and the thickness of the dielectric ~ 2 µm. Approximations with a power law result in a high value of the exponent, $m > 4$. In Schottky coordinates the I-V characteristic can be approximated with two lines having a slope decreasing approximately two times at large voltages (above ~35 V). This might indicate different conduction mechanisms at low and high electrical fields in the dielectric.

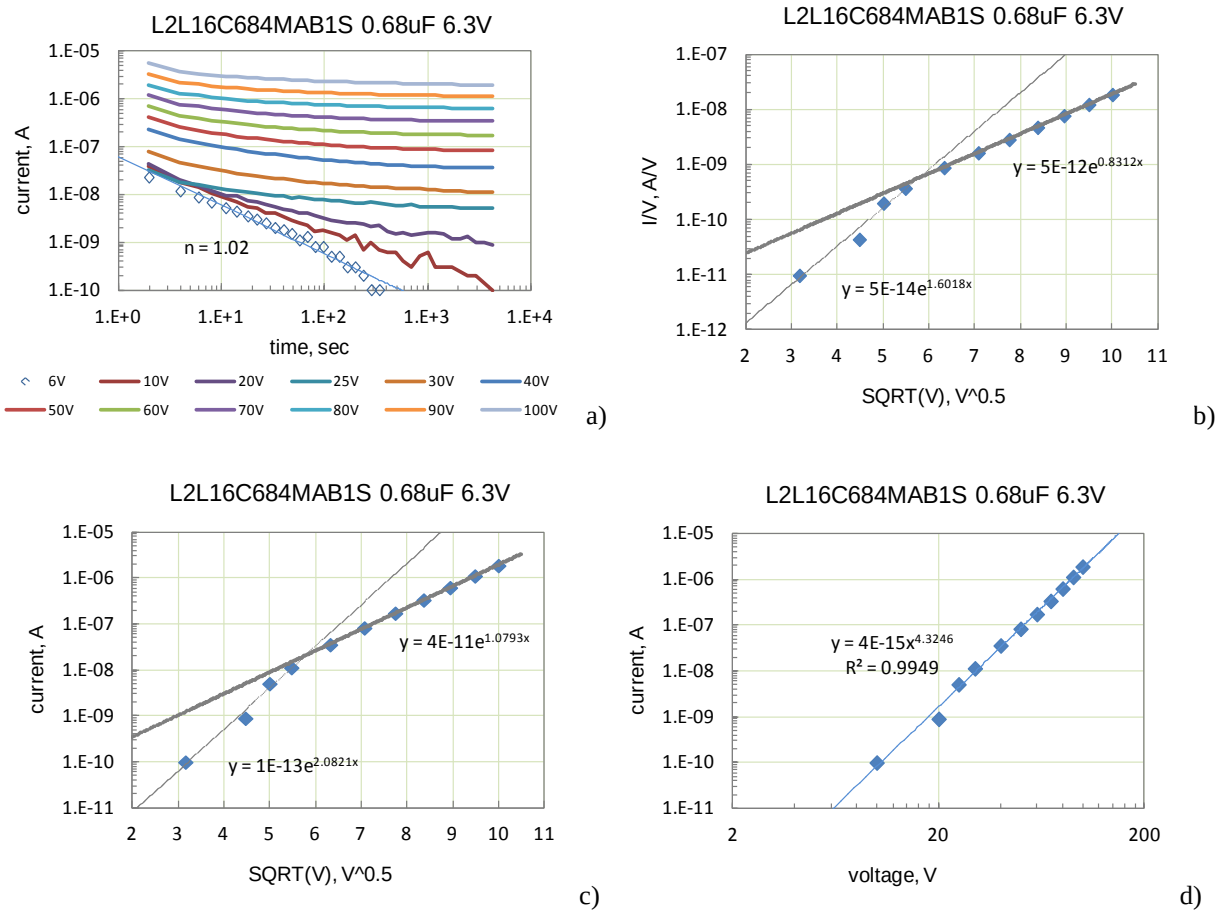

Figure 4.7. Transient currents in a 0.68 µF 6.3V interdigitated capacitor (IDC) used in XILINX FPGAs (a) and its I-V characteristics in Poole-Frenkel (b), Schottky (c) and double logarithmic coordinates (d).

V. Effect of temperature on absorption and leakage currents

Currents measured at rated voltages and temperatures varying from room (300 K) to cryogenic (200 K and 36 K) in X5R 100 µF 6.3 V and 47 µF 16 V that were manufactured by two vendors had similar amplitudes and decay rates (see Figure 5.1). This indicates that absorption currents have a weak dependence on temperature.

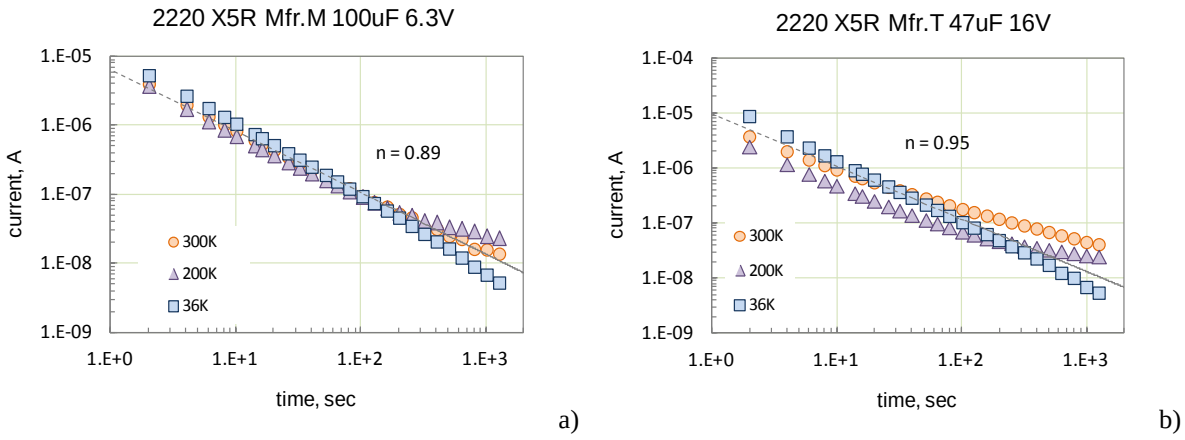

Figure 5.1. Current relaxation at room and cryogenic temperatures (200 K and 36 K) for 100 μF 6.3 V (a) and 47 μF 16 V (b) X5R capacitors.

A similar conclusion can be made based on analysis of polarization and depolarization currents in different types of 1206 X7R capacitors shown in Figure 5.2. Depolarization currents measured at temperatures from room to 165 °C remained practically the same, whereas leakage currents under rated voltages dominate at temperatures 85 °C and above so absorption currents became negligible already after a few seconds of polarization.

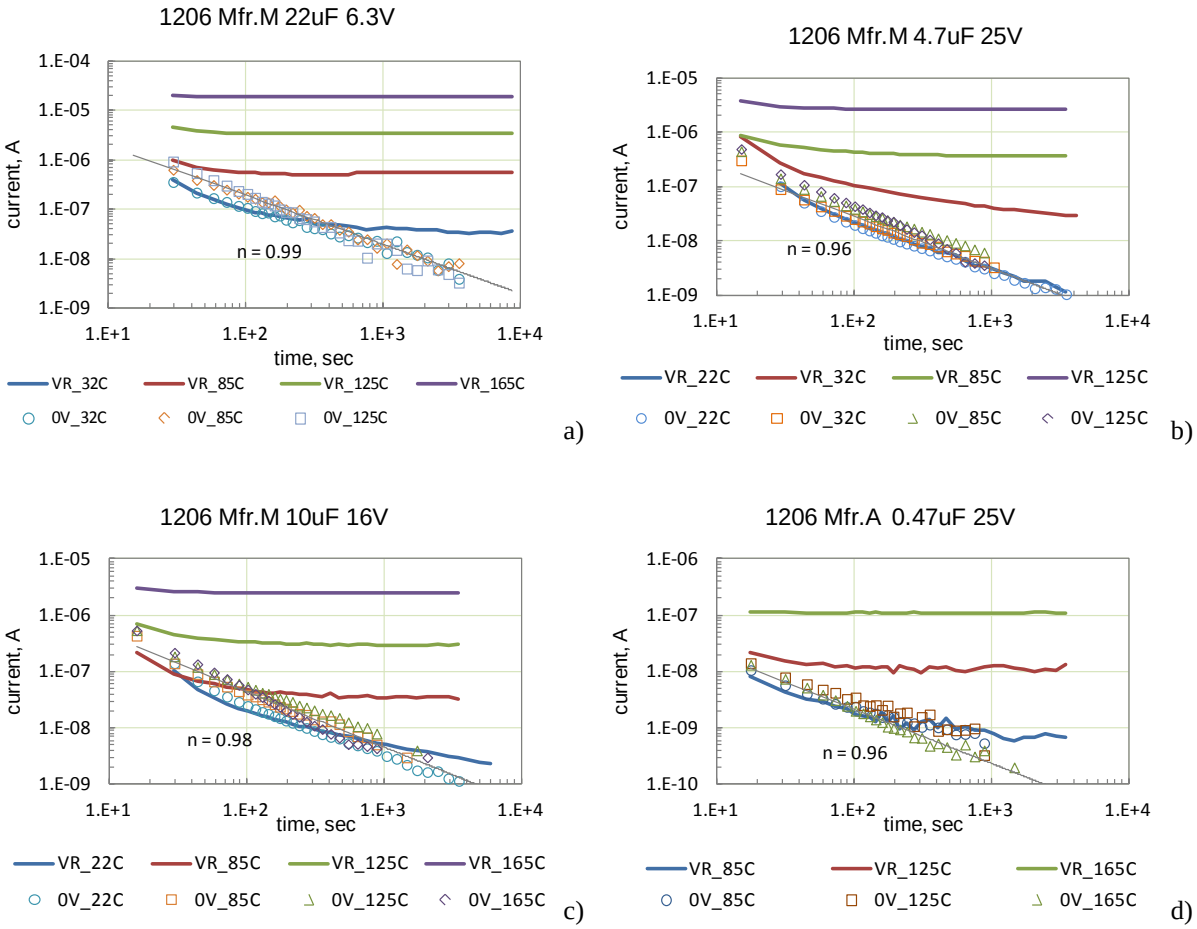

Figure 5.2. Relaxation of polarization (lines) and depolarization (marks) currents in four 1206 X7R capacitors at temperatures from room to 165 °C.

I-V characteristics of four types of 1206 capacitors presented in Figure 5.2 are plotted in double logarithmic and Schottky coordinates in Figure 5.3. Similar to previous results, the data can be approximated with straight lines equally well in both cases. Approximation of I-V curves with a power law results in the value of exponents *m* varying from 1.3 to 2.5 and the slope of I-V curves plotted in Schottky coordinates varied from 0.8 to 1.4.

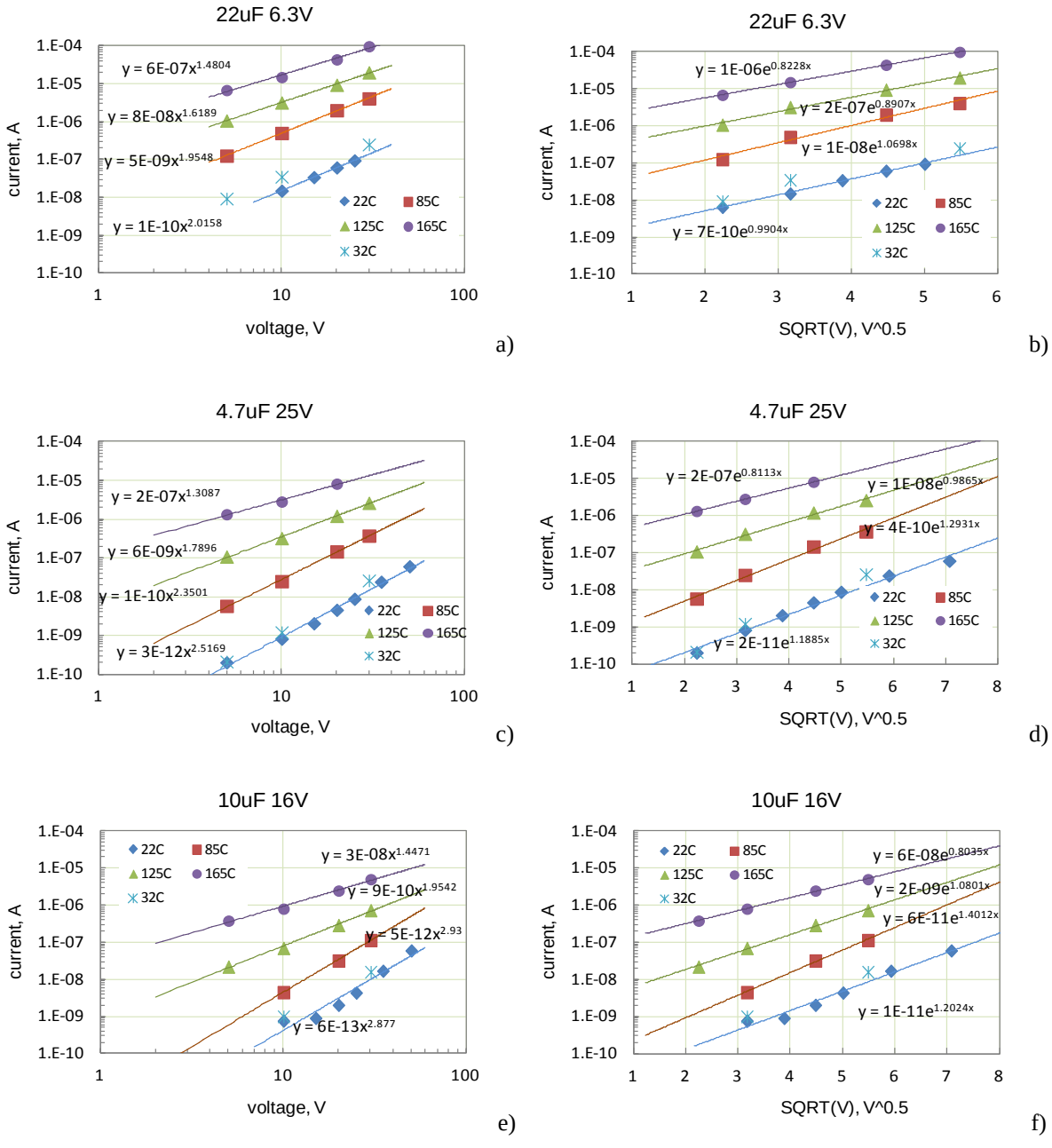

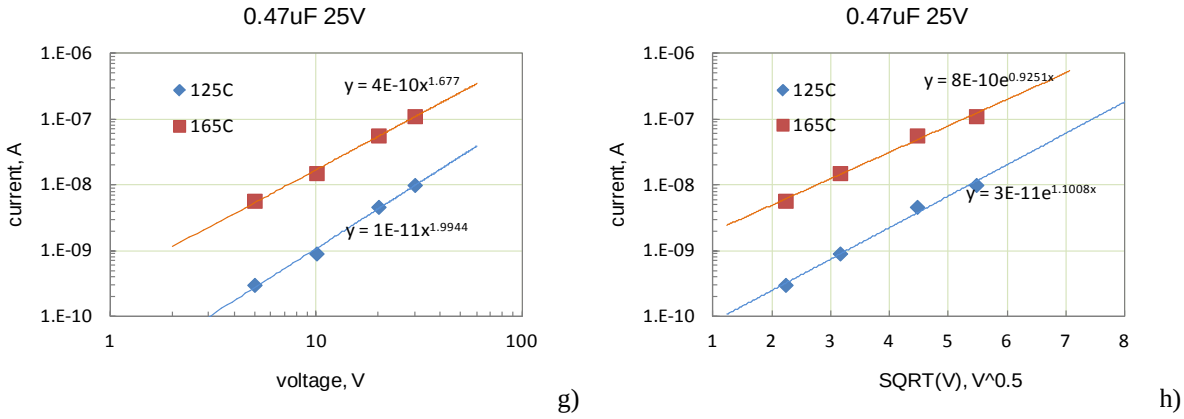

Figure 5.3. I-V characteristics of 1206 X7R capacitors in double logarithmic (a, c, e, g) and Schottky (b, d, f, h) coordinates.

Temperature dependence of the exponent *m* calculated as a slope of I-V curves in double logarithmic coordinates is shown in Figure 5.4. At relatively low temperatures, below 85 °C *m* does not change substantially, and depending on the part type is in the range from 2, to 2.7. At higher temperatures the exponent decreases almost linearly to a level of ~ 1.5 at 165 °C.

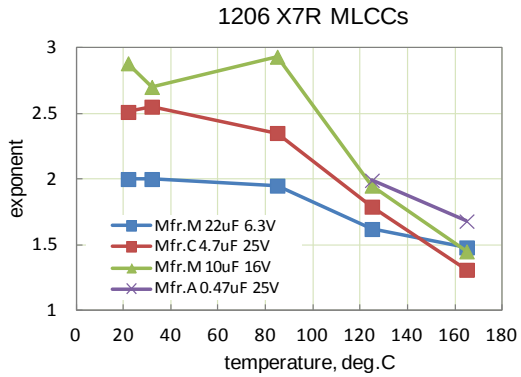

Figure 5.4. Variations of the exponent *m* with temperature for different X7R capacitors.

Temperature dependencies of currents at different voltages are shown in Figure 5.5. In Arrhenius coordinates the experimental data can be accurately enough approximated with straight lines with a slope indicating the activation energy, E_a, of leakage currents (or insulation resistance). In all cases the slope decreases as voltage increases indicating a decrease in activation energy (see Figure 5.6.) At relatively low voltages the activation energy for different part types varies from 0.55 eV to 1 eV and decreases by 10% to 30% as the voltage increases from 5 V to 30 V.

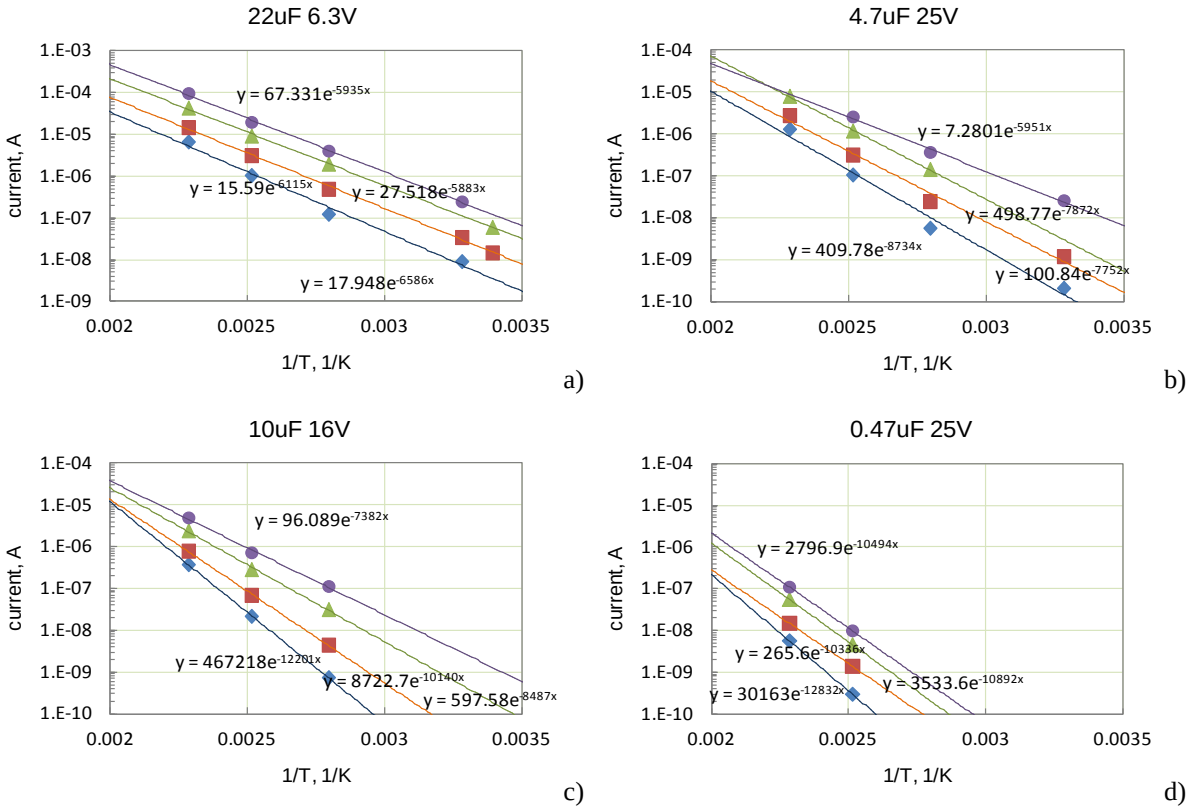

Figure 5.5. Temperature dependence of leakage currents at different voltages for four 1206 X7R capacitors in Arrhenius coordinates.

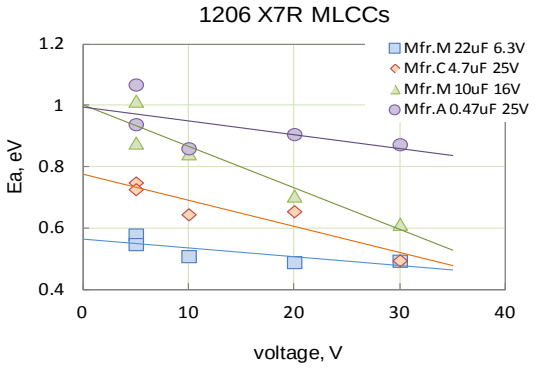

Figure 5.6. Variation of activation energy with voltage for 4 types of X7R capacitors.

For three types of 1 µF 50 V relatively large-size capacitors (EIA size code 2220 and 2225) manufactured by different vendors currents were measured in the range of voltages from 5 V to 150 V at temperatures in the range from 125 °C to 182 °C (the temperature was limited by the eutectic Sn/Pb solder used). Results of these measurements are shown in Figures 5.7 to 5.9. As can be seen in plots presenting I-V characteristics in double logarithmic coordinates the power function fits well the data, and the exponent *m* varies in a relatively narrow range from 1.42 to 1.56 for all part types. Attempts to straighten the data in Schottky coordinates showed that the slopes of curves at low voltages (below VR) are much greater than at high voltages.

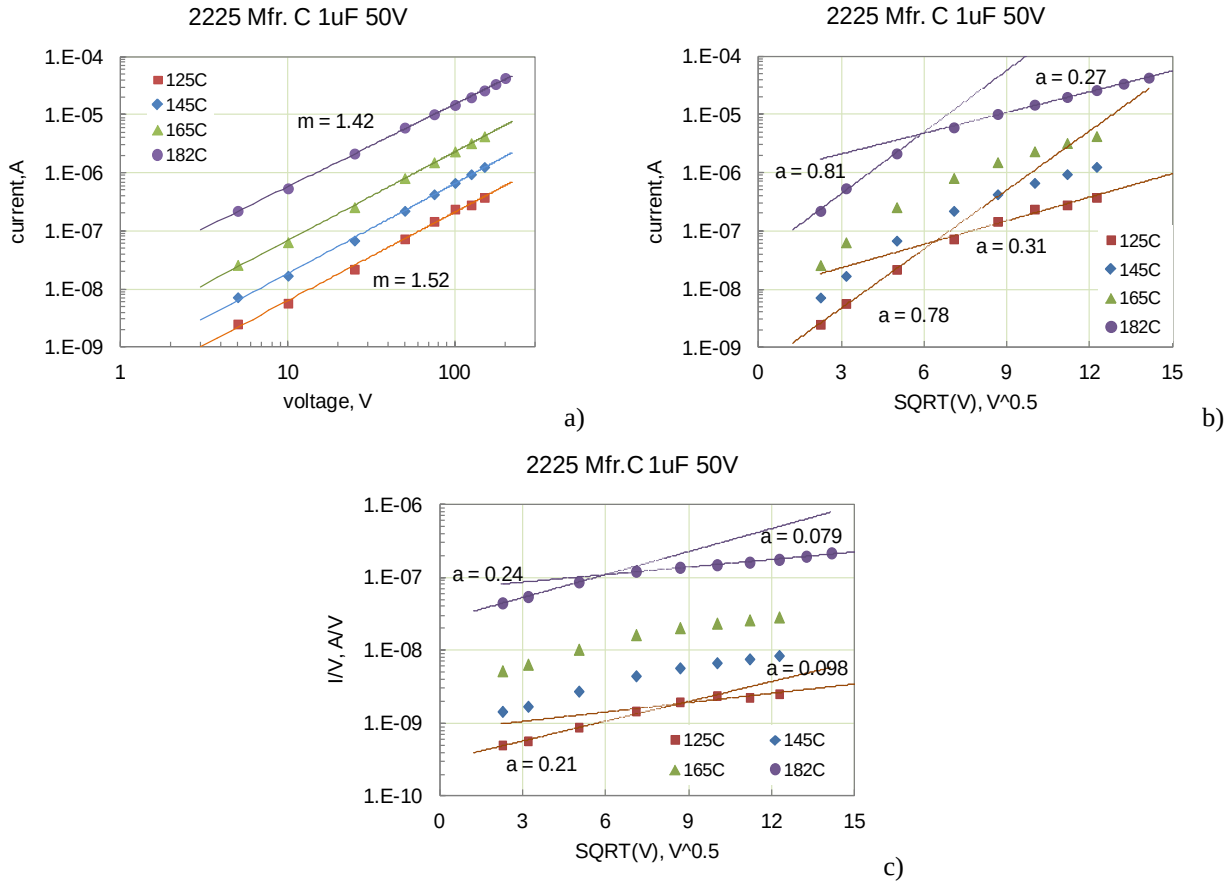

Figure 5.7. I-V characteristics of 1 µF 50 V capacitors from manufacturer C at high temperatures, from 125 °C to 182 °C in double logarithmic (a). Schottky (b) and Poole-Frenkel (c) coordinates.

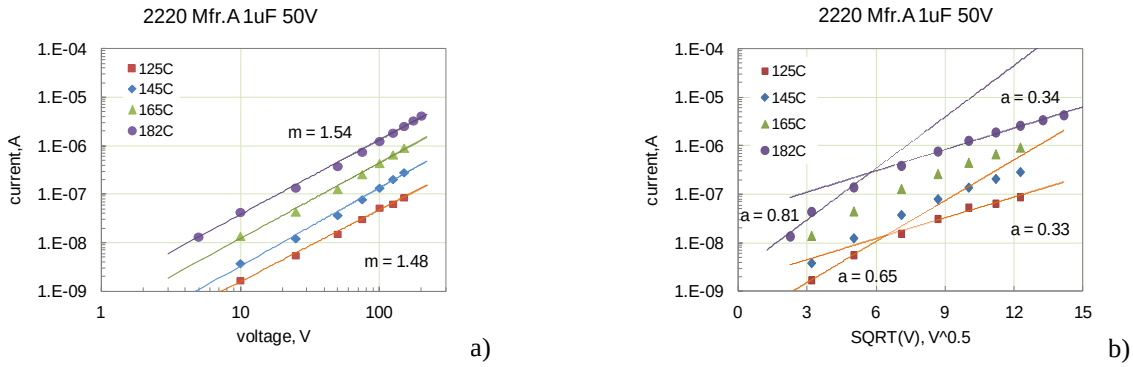

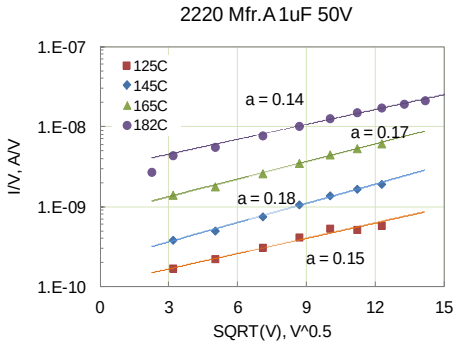

c)

Figure 5.8. I-V characteristics of 1 μF 50 V capacitors from manufacturer A at high temperatures, from 125 °C to 182 °C in double logarithmic (a). Schottky (b) and Poole-Frenkel (c) coordinates.

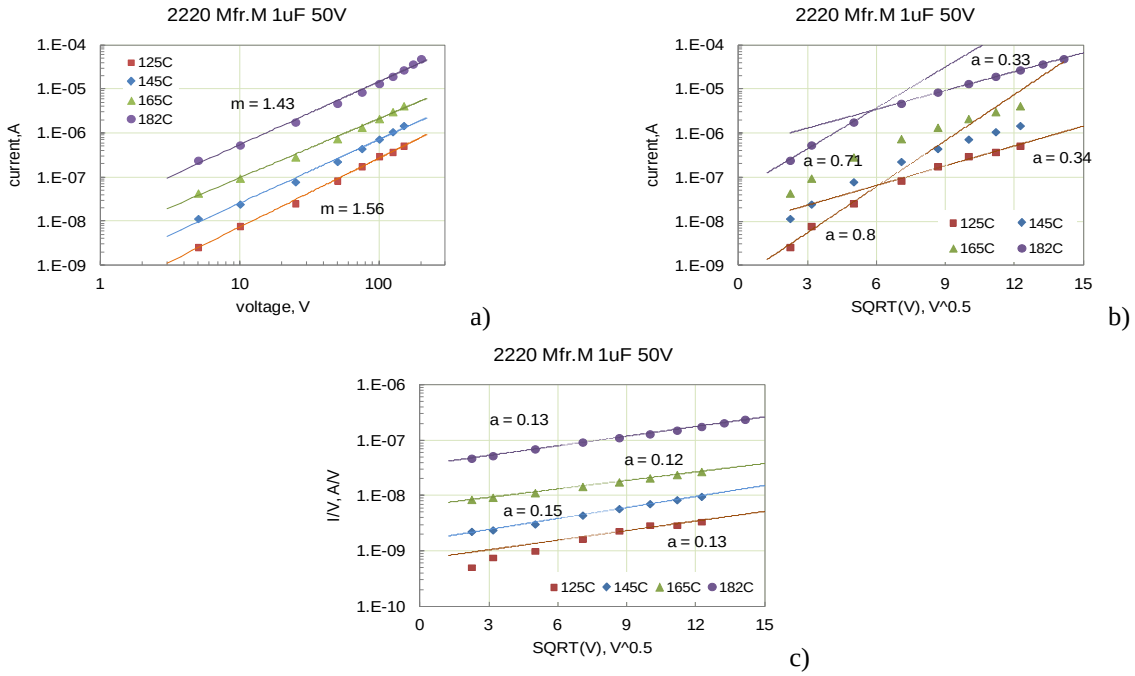

Figure 5.9. I-V characteristics of 1 μF 50 V capacitors from manufacturer M at high temperatures, from 125 °C to 182 °C in double logarithmic (a). Schottky (b) and Poole-Frenkel (c) coordinates.

Temperature dependencies of currents measured at 10 V and 150 V for the three parts are shown in Arrhenius coordinates in Figure 5.10. For capacitors from Mfr.A the value of E_a did not change substantially with voltage remaining at ~0.87 eV. For two other part types E_a decreased from 1.17 eV at 10 V to 1 eV at 150 V.

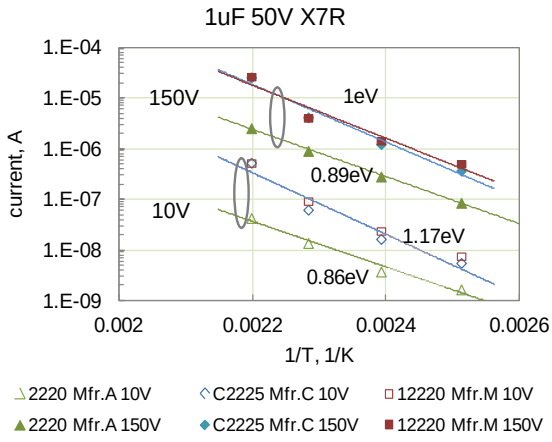

Figure 5.10. Temperature dependence of leakage currents in three different 1 μF 50 V capacitors in Arrhenius coordinates.

VI. Effect of cracking on absorption and leakage currents

Polarization and depolarization currents were measured on a variety of normal (virgin) ceramic capacitors and capacitors with cracks formed by one of the techniques described in section II. Results of these measurements at room temperature are shown in Figures 6.1 to 6.4.

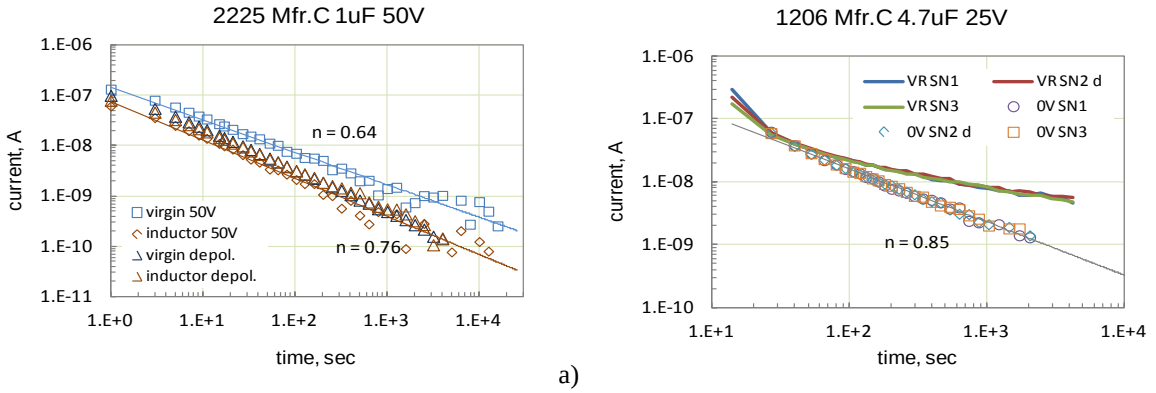

Figure 6.1. Polarization and depolarization currents in virgin X7R capacitors and parts damaged by the Vickers inductor.

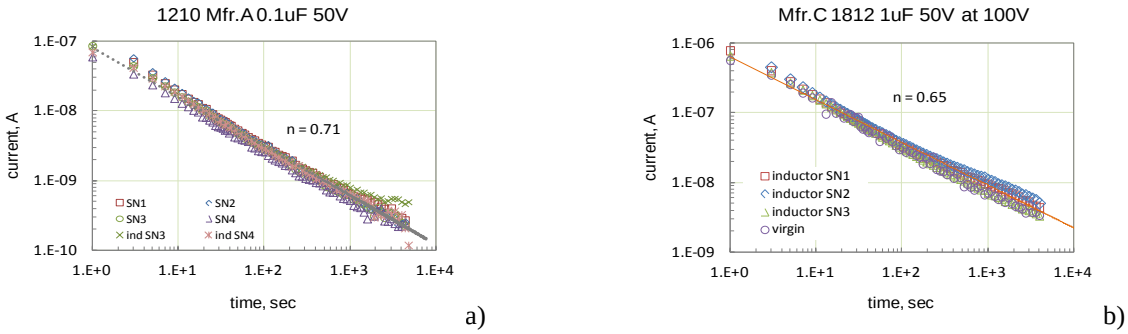

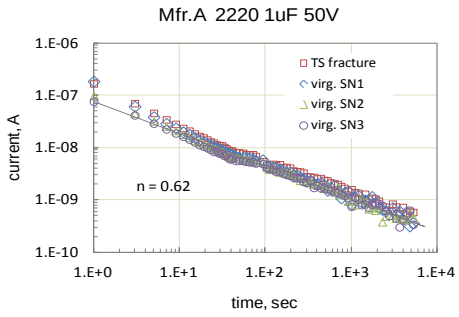

c)

Figure 6.2. Relaxation of currents in normal and fractured X7R capacitors. One part shown in figure (c) was fractured by thermal shock, and parts in two other groups were damaged by the inductor.

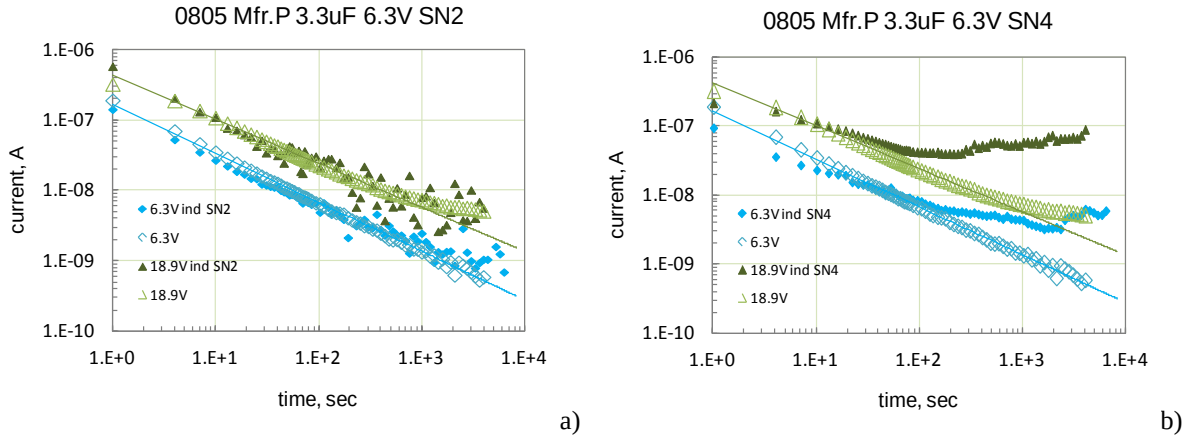

a) b)

Figure 6.3. Polarization and depolarization currents in two samples of virgin and damaged by the Vickers inductor 3.3 μF 6.3 V X7R capacitors.

In all cases, except SN4 of 3.3 μF 6.3 V capacitor (Figure 6.3.b) absorption currents (both, polarization and depolarization) were similar for virgin and damaged parts. At the rated voltage, leakage currents exceeded absorption currents for SN4 after 120 seconds of electrification, so even this capacitor most likely would not be detected by the IR screening. At higher voltages (3VR) the presence of a defect in SN4 is more obvious, but even at these conditions abasorption currents prevail up to ~ 60 sec of electrification.

An interesting phenomenon was observed in several cases where absorption currents were slightly larger in capacitors with cracks compared to virgin parts. Examples of these cases are shown in Figure 6.4. Typically, the presence of cracks is expected to increase leakage currents that would appear on the *I-t* cerves as eary leveling-off similar to what is shown in Figure 6.3.b. However, in cases shown in Figure 6.4 the rate of current decay in damaged capacitors is not changing substantially compared to virgin parts, whereas isocronic currents increased noticeably.

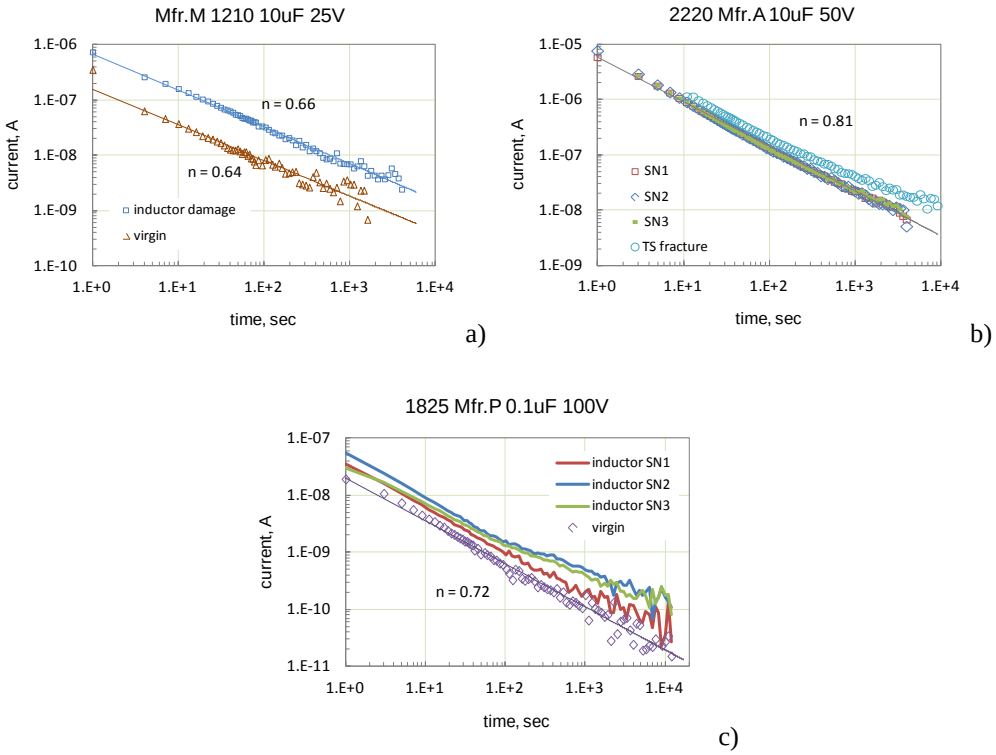

Figure 6.4. Relaxation of currents in normal and fractured X7R capacitors. One part shown in figure (b) was fractured by thermal shock, and parts in two other groups were damaged by the Vickers inductor. Note that absorption currentas in damaged capacitors are larger that in virgin parts.

Due to anomalies in the manufacturing process, one experimental lot of 82 nF 50V X7R capacitors had multiple voiding and delaminations that were revealed by acoustic microscopy and cross-sectioning (see Figure 6.5). This defective lot was used to evaluate the sensitivity of IR measurements to the presence of internal defects in MLCCs. Figure 6.5.a shows that absorption currents in capacitors from defective and normal lots were similar and no leakage currents were observed even after several hours of electrification. It is interesting to note that this defective lot passed IR testing at 125 °C with all parts having IR exceeding 10^{10} ohm, and voltage conditioning test at 125 °C. A group of 15 samples was tested by highly accelerated life testing, HALT, at 125 °C and 150 V for 200 hours and had no failures. Apparently, closed internal voids are not increasing leakage currents substantially.

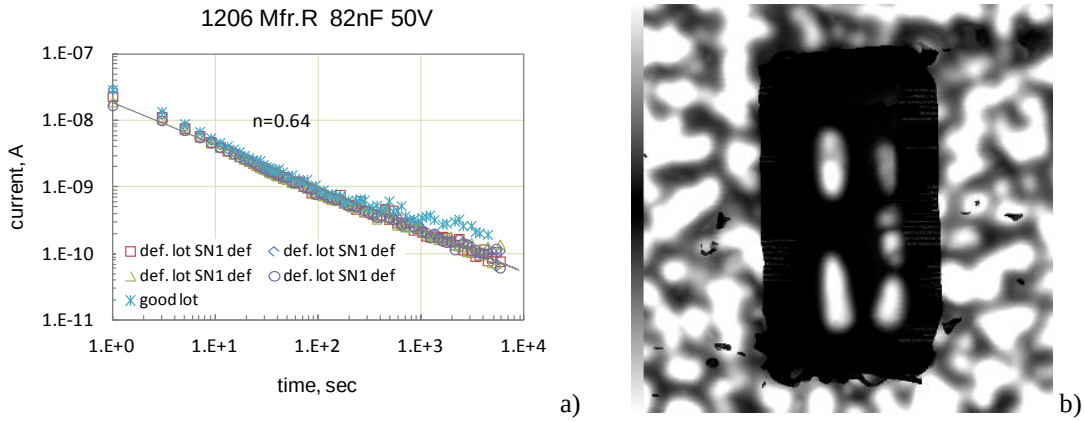

c)

Figure 6.5. Comparison of current relaxation in capacitors from defective and normal lots (a). Figures b) and c) show an acoustic image and cross-sectional view of a capacitor from the defective lot.

Leakage currents in several types of 1206 X7R virgin and fractured capacitors were measured over a wide range of voltages and temperatures. Results of these measurements are shown in Figures 6.6 and 6.7 and indicate that increase in temperature up to 165 °C does not allow revealing the presence of mechanical defects in MLCCs. This is due to a high level of intrinsic leakage currents in high-value capacitors that obviously exceeds the level of currents related to the presence of cracks.

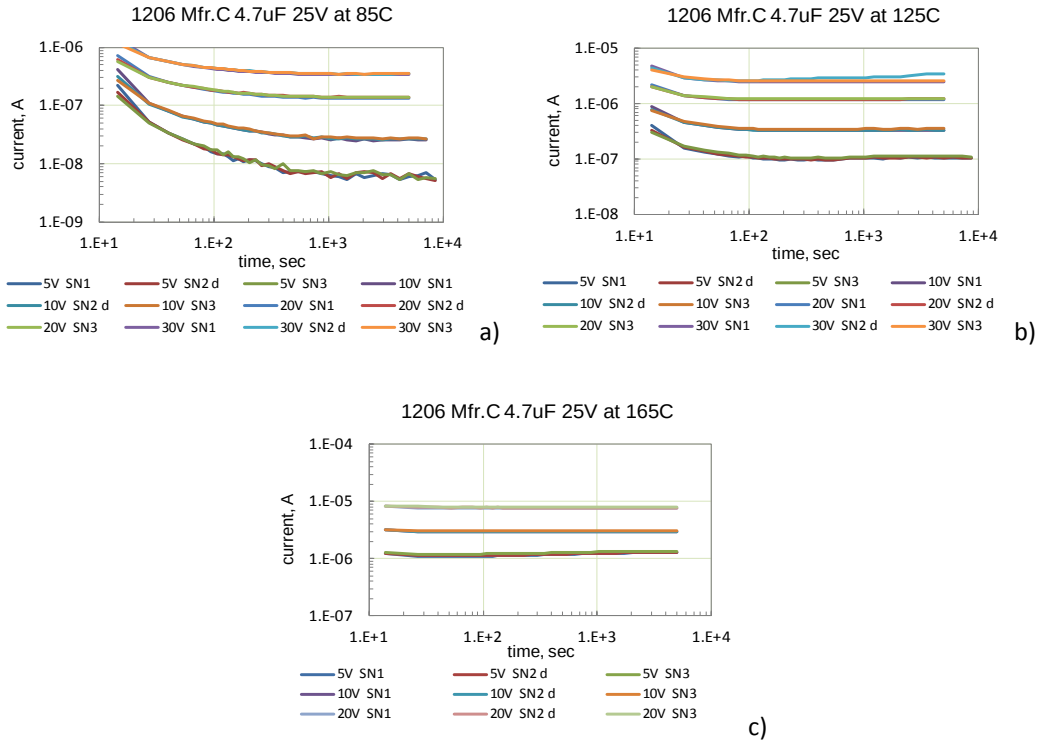

Figure 6.6. Currents in two normal and one damaged by inductor (SN2) 4.7 µF 25 V capacitors at 85 °C (a), 125 °C (b), and 165 °C (c) and different voltages.

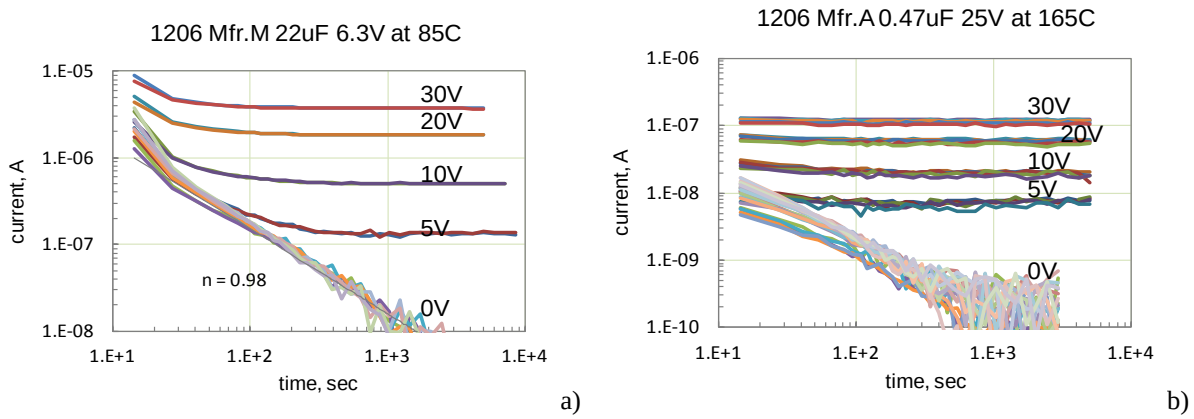

Figure 6.7. Polarization and depolarization currents in 22 μF 6.3 V (a) and 0.47 μF 25 V capacitors at 85 °C (a) and 165 °C (b). Out of two parts tested in the first group one was damaged with a Vickers inductor and another used as a reference. Two parts out of five measured in the second group had inductor-induced cracks.

VII. Absorption capacitance

If a charge, Q_t, that is transferred into the dielectric during poling, increases with voltage linearly, the absorption process can be described by a capacitance C_t that is determined as

$$C_t = \frac{Q_t}{V}$$

The value of Q_t can be calculated by integrating absorption currents with time. Assuming that the absorption current decreases with time according to a power law, Eq.(1.2), Q_t can be expressed as:

$$Q_t = \int_1^{1000} I_0 \times t^{-n} \times dt = \frac{I_0}{1-n} \times t^{1-n}\Big|_1^{1000} \quad \text{at n} \neq 1 \text{ and} \qquad (7.1)$$

$$Q_t = I_0 \times \ln(t)\Big|_1^{10000} \quad \text{at n} = 1$$

Based on results reported above, the relationship Eq.(1.2) is valid within the period from seconds to several hours, and for this reason the integration limits were chosen from 1 sec to 10,000 sec. To assess how significant the effect of time range on Q_t is, normalized values of the absorption charge, Q_t/I_0, were calculated from 1 sec to 10 ksec and from 1 sec to 100 ksec. Results of these calculations are shown in Figure 7.1. At n > 1 the difference in Q_t is negligible, and even at relatively low values of n it is much less than an order of magnitude, e.g. at n = 0.7 the charge increases two times only. This means that variation in the time limit will not change Q_t values dramatically.

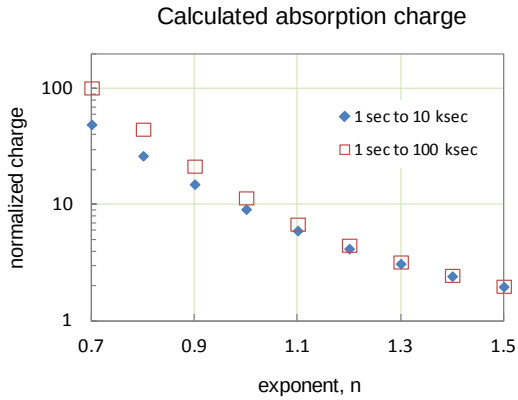

Figure 7.1. Variations of the calculated per Eq.(7.1) normalized charges vs. exponent *n* for two time periods: from 1 sec to 10 ksec and from 1 sec to 100 ksec.

Figure 7.2 shows variation of absorption charge with voltage for 10 types of different types of X5R and X7R capacitors. Values of Q_t were calculated using Eq.(7.1) in the range from 1 sec to 10 ksec based on parameters *n* and I_0 obtained by approximation of experimental *I-t* characteristics. For these parts Q_t varies linearly up to voltages exceeding the rated voltage 2 to 3 times. In all cases the experimental data follow linear relationships with the slopes corresponding to the value of absorbed charge capacitance.

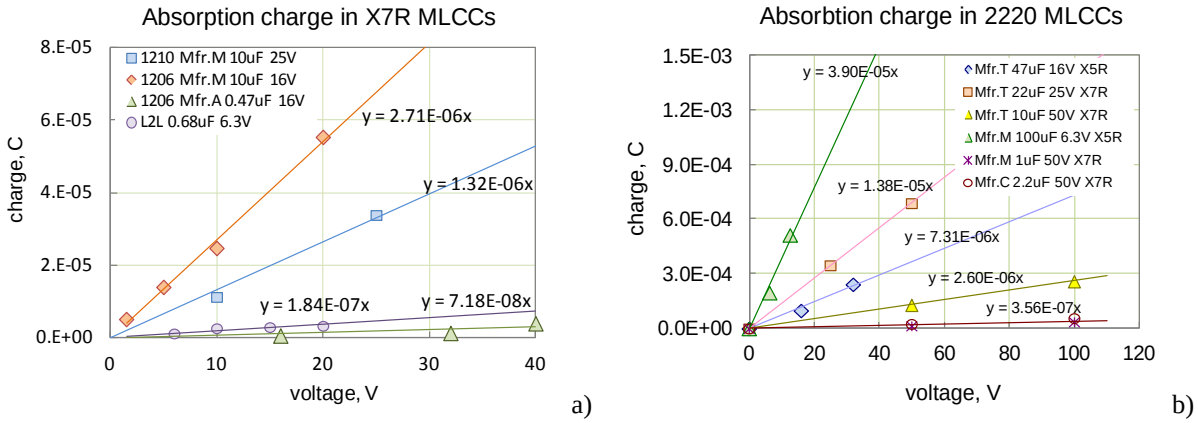

Figure 7.2. Variations of absorption charges with applied voltage. Absorption charges were calculated using Eq.(7.1) based on I-t characteristics measured at different voltages.

For several large value capacitors the absorption charges saturated at voltages exceeding VR (see Figure 7.3). For these cases the value of C_t was estimated based on the slope of Q_t-*V* curves at low voltages. Absorption capacitance is greater for capacitors of larger values and there is a correlation between C_0 and C_t (see Figure 7.4.). On average, C_t value is approximately 25% to 30% of the nominal value for most tested X7R capacitors. However, for COG capacitors the value of absorption capacitance is much less (see Figure 7.3.b) and comprises ~ 3% of C_0.

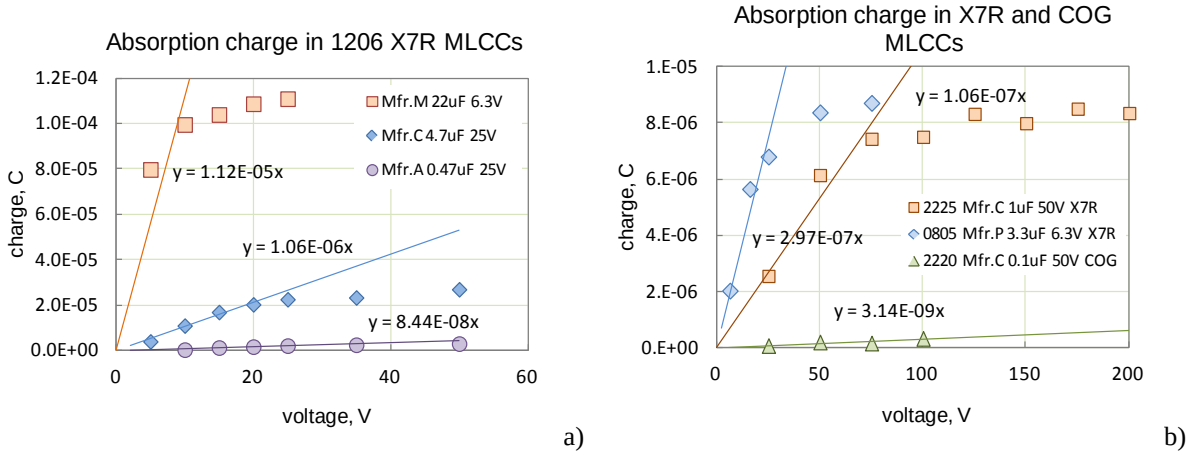

a) b)

Figure 7.3. Variations of absorption charges with applied voltage in X7R 1206 capacitors (a) and comparison of absorption charges in X7R and COG capacitors (b).

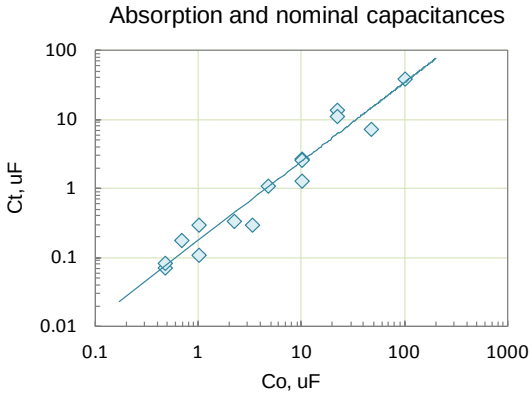

Figure 7.4. Correlation between the absorption and nominal values of capacitance for 15 different types of X7R MLCCs.

Results of C_t calculations for 30 different types of X5R and X7R capacitors are shown in Table 7.1. For two types of 10 µF 25 V capacitors from Mfr.T (#15 and #16) the values of C_t were substantially larger than the nominal values; however, in all other cases the average C_t/C_0 ratio was ~ 0.29 at a standard deviation of 0.16.

A simple constant current stress (CCS) testing allows for estimations of the direct current capacitance, C_{DC}, of the parts. During CCS testing a constant current, I_s, typically in the microampere range, is forced into a part while the voltage across the capacitor is monitored using a source measure unit (SMU), in our case Keithley-236/7. Under these conditions, the voltage increases linearly with time, and the slope of *V-t* curves allows for calculations of C_{DC}:

$$V(t) = \frac{I_s \times t}{C_{DC}}$$

Table 7.1. Absorption capacitance in different types of X7R and X5R MLCCs.

#	EIA size	Mfr.	C_0, µF	VR, V	Dielectric	Ct_I-t, µF	Ct/Co, µF
1	0402	C	0.01	6.3	X7R	0.0036	0.36
2	0508	A	0.68	6.3	X7R	0.072	0.11
3	0805	Pa	0.1	50	X7R	0.034	0.34
4	0805	N	0.1	50	X7R	0.017	0.17
5	0805	C	0.1	50	X7R	0.035	0.35
6	0805	A	0.12	50	X7R	0.043	0.36
7	CDR31 (0805)	A	0.018	50	X7R	0.014	0.78
8	1206	M	10	16	X7R	2.71	0.27
9	1206	M	22	6.3	X5R	11.2	0.55
10	1206	M	10	16	X7R	1.47	0.15
11	1206	C	4.7	25	X7R	1.1	0.23
12	1206	A	0.47	25	X7R	0.085	0.18
13	1206	R	0.082	50	X7R	0.028	0.34
14	1210	M	10	25	X7R	1.32	0.13
15	1210	T	10	25	X7R	17.8	1.78
16	1210	T	10	25	X7R	14.5	1.45
17	1812	A	1	50	X7R	0.3	0.30
18	1812	C	1	50	X7R	0.35	0.35
19	1825	C	1	50	X7R	0.25	0.25
20	CDR35 (1825)	C	0.1	100	X7R	0.012	0.12
21	2220	M	100	6.3	X5R	39	0.39
22	2220	T	22	25	X7R	13.8	0.63
23	2220	T	47	16	X5R	8.3	0.18
24	2220	M	1	50	X7R	0.35	0.35
25	2220	T	10	50	X7R	2.6	0.26
26	2220	C	1	50	X7R	0.2	0.20
27	2220	A	1	50	X7R	0.13	0.13
28	2220	A	10	50	X7R	3	0.30
29	2225	C	2.2	50	X7R	0.36	0.16
30	2225	C	1	50	X7R	0.11	0.11

Variations of voltages with time during CCS testing for several part types are shown in Figure (7.5.) At voltages below VR the curves can be approximated with straight lines; however, the slope increases substantially at higher voltages due to a decrease in capacitance.

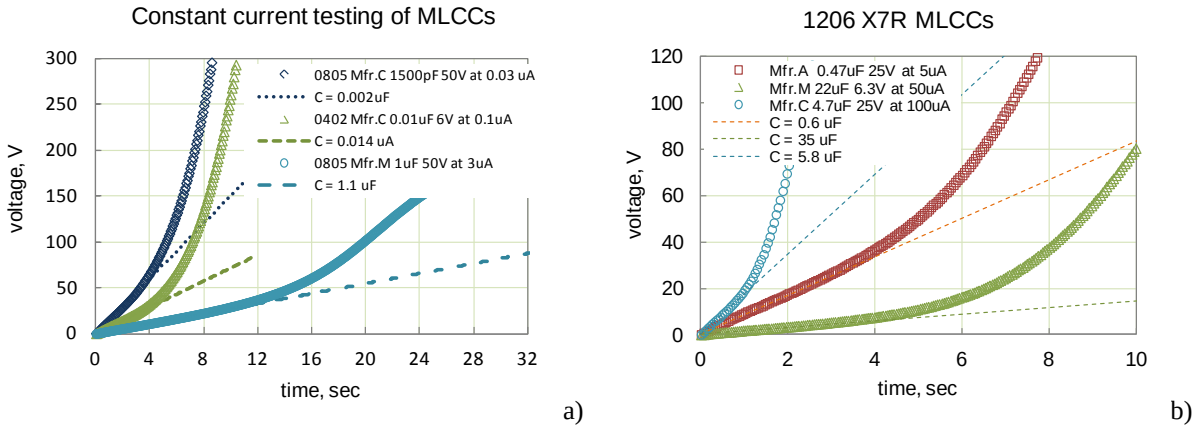

Figure 7.5. Constant current stress testing for different types of X7R capacitors.

Correlation between C_t and capacitance calculated based on CCS testing, C_{DC}, is shown in Figure 7.6.a. In most cases CCS measurements resulted in slightly smaller values of capacitance. Values of C_{DC}

normalized to the nominal values, C_0, are only ~5% less than C_t/C_0, thus indicating that both, *I-t* and *V-t*, techniques that are based on DC measurements result in close values of capacitance. Figure 7.6.b shows correlation between C_{DC} and the value of capacitance measured at 1 kHz. In all cases C_{DC} exceeds C_1kHz on approximately 23%.

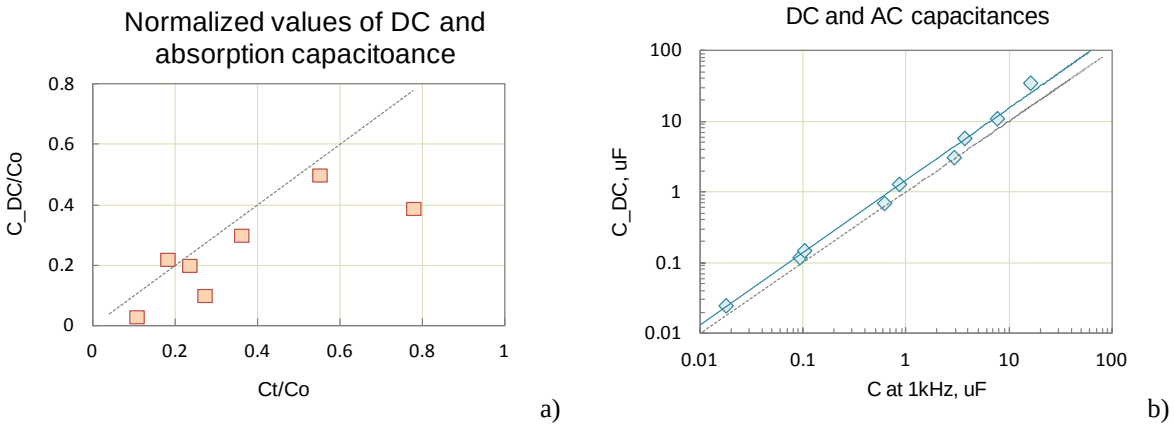

Figure 7.6. Correlation between normalized values of capacitance measured at direct current conditions based on *V-t* characteristics, C_{DC}, and capacitance determined based on absorption current measurements, *I-t* characteristics (a) and between C_{DC} and capacitance measured at 1 kHz (b). Dashed lines on both charts correspond to no-change values.

VIII. Modeling of absorption currents

An equivalent circuit of a capacitor with a nominal value C_0 and insulation resistance R that accounts for the effects related to dielectric absorption was suggested first for polystyrene capacitors by Dow in 1958 [21] and is presented in Figure 8.1. Dow showed that most absorption polarization processes in capacitors can be described using a circuit with five *R-C* relaxators connected in parallel to C_0 by a proper selection of the relaxation times $\tau_i = R_i \times C_{ti}$ and absorption capacitances C_{ti}. Note that the high-frequency capacitance of this circuit is equal to C_0, and the DC capacitance (at zero frequency) is $C_0 + \Sigma C_{ti}$.

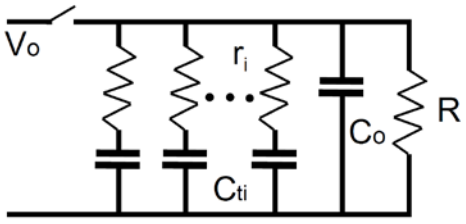

Figure 8.1. Dow model of a capacitor.

If a step voltage V_0 is applied at $t = 0$, than variations of the current with time can be given by a simple equation:

$$I(t) = \frac{V_0}{R} + \sum_i \frac{V_0}{r_i} \exp\left(-t/\tau_i\right) \qquad (8.1)$$

Below we'll show that the empirical Curie von Schweidler law and most experimental data of absorption currents in MLCCs can be simulated using a simple four-element circuit and the exponent n in Eq.(1.2) can vary substantially depending on the distribution of τ_i and C_{ti}. For simplicity, let us consider a 4.7 μF 16 V capacitor with a high insulation resistance, so the leakage current (the first element in Eq.8.1) is negligible compared to the absorption currents. Assuming all C_{ti} equal to 1 μF and τ_i increasing an order of magnitude from τ_1 = 100 sec to τ_4 = 100 ksec, a decay of the total absorption current that is a superposition if currents in individual relaxators can be approximated with a power law, $I \sim t^{-1.02}$, in the range of times from 100 sec to 100 ksec (see Figure 8.2.a). If absorption capacitance increases in relaxators having larger resistance, as it is shown in Figure 8.2.b, than the slope of absorption current decreases, e.g. if $C_{ti} = i \times 1$ μF and the values of r_i remain the same as in the previous case, the exponent $n = 0.83$. By decreasing absorption capacitances for relaxators with larger resistances, $C_{ti} = 0.33 \times C_{ti-1}$, the rate of the current decay can increased. For example, as shown in Figure 8.2.c, a three times decrease of C_{ti} for relaxators with larger level of resistance r_i, results in a current relaxation with the exponent n = 2.

Obviously, by adding more *R-C* relaxators in the circuit shown in Figure 8.1 with characteristic times below 100 sec of greater than 100 ksec, the applicability of the Curie van Schwendler law can be extended to a larger range of times. A physical interpretation of this model will be considered in the discussion section of the report.

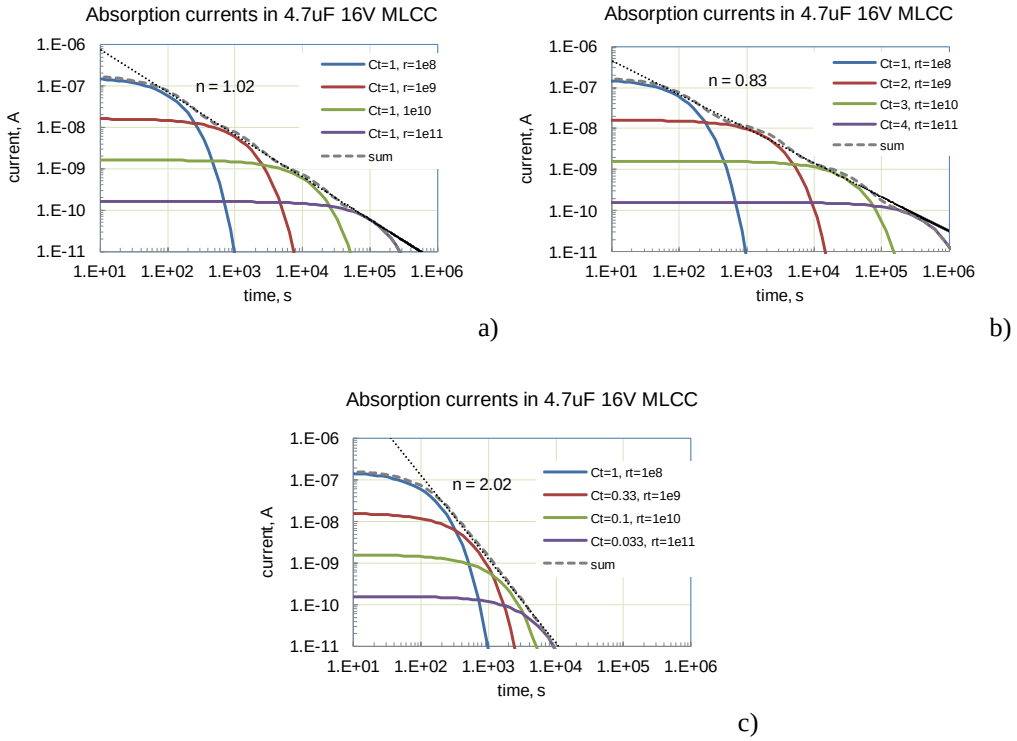

Figure 8.2. Simulation of absorption currents in 4.7 μF 16 V capacitors using an equivalent circuit with four relaxators having the same values of r_i but different distributions of absorption capacitance. C_{ti} is constant in figure (a), increases for relaxators with larger r_i in figure (b), and decreases in figure (c).

IX. Modeling of absorption voltages

If a capacitor that is modeled by a circuit shown in Figure 8.1 remains under bias for a long period of time that exceeds maximum characteristic time τ_i, then each of the capacitors C_{ti} will be charged to V_0. Shorting such a capacitor for a period of Δt will discharge only C_0 and capacitors C_{ti} associated with relatively fast *R-C* relaxators that have $\tau_i < \Delta t$. All other capacitors will remain charged and when the circuit is open these charges will leak out to C_0 and increase the voltage across the capacitor. This voltage will increase with time till discharging currents through the leakage resistor *R* prevail thus resulting in the voltage roll-off. The absorption voltage, V_{abs}, will decrease with time, and eventually the capacitor discharges completely. The initial period of the process, when voltage is increasing with time is described as so-called dielectric absorption phenomena. At relatively large insulation resistances and relatively small times after open circuit, variations of the absorption voltage do not depend on *R* and the process is not sensitive to the presence of defects in capacitors. However, decreasing of V_{abs} with time is controlled by the value of *R* and for this reason the following analysis is focused on relatively long-term processes occurring during and after the voltage roll-off.

When absorption voltage is decreasing with time, the process is scaled to the characteristic time related to the insulation resistance R, $\tau_0 = R \times C_0$. By this time relaxators with $\tau_i << \tau_0$ will be mostly discharged onto C_0, and considering that the charging period is less than τ_0, relaxators with $\tau_i >> \tau_0$ are not charged and will not contribute substantially to the discharging process. For this reason we can simplify the equivalent circuit by considering only relaxators having timing characteristics τ_i that are close to the duration of polarization.

Let us consider a schematic of a capacitor shown in Figure 9.1 that had been precharged for some time and then short circuited briefly. At the end of the precharge period the voltage across capacitor C_t was U_0 and due to a high value of resistor *r* it did not change substantially during the short circuit period. After short circuit, capacitor C_t is discharging at a rate that corresponds to a current i_1 and capacitor C_0 is charging at a rate that corresponds to current i_2. Current i_3 is a leakage due to the intrinsic conductivity of the dielectric or due to defects in the capacitor that can be characterized by a resistor *R*.

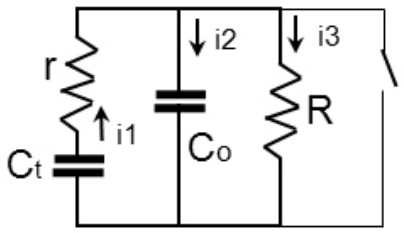

Figure 9.1. Model for calculations of absorption voltages.

The currents in this circuit obey the first Kirchhoff's law:

$$i_1 = i_2 + i_3, \qquad (9.1)$$

and can be expressed as follows:

$$i_1 = -C_t \frac{du}{dt}, \quad i_2 = C_0 \frac{dv}{dt}, \quad i_3 = \frac{v}{R}. \qquad (9.2)$$

Here *u(t)* is the voltage across capacitor C_t, and *v(t)* is the absorption voltage, or voltage across C_0.
The balance of currents, Eq.(9.1), can be written as:

$$-C_t \frac{du}{dt} = C_0 \frac{dv}{dt} + \frac{v}{R} \ , \qquad (9.3)$$

The voltage across C_0 is less than across C_t due to a voltage drop across the resistor *r*:

$$v(t) = u(t) - i_1 \times r \ . \qquad (9.4)$$

After a substitution for currents per Eq.(9.2) the derivative of Eq.(9.1) and Eq.(9.4) can be presented as:

$$\frac{d^2u}{dt^2} = -\frac{1}{C_t R}\frac{dv}{dt} - \frac{C_0}{C_t}\frac{d^2v}{dt^2} \ , \qquad (9.5)$$

$$\frac{dv}{dt} = C_t \times r \times \frac{d^2u}{dt^2} + \frac{du}{dt}, \qquad (9.6)$$

Substitution of Eq.(9.3) and Eq.(9.5) into Eq.(9.6) gives an equation for the absorption voltage:

$$a\frac{d^2v}{dt^2} + b\frac{dv}{dt} + c \times v = 0 \, , \qquad (9.7)$$

where

$$a = \tau_0 \frac{\tau}{\tau_t} \ , \quad b = \frac{\tau + \tau_t + \tau_0}{\tau_t} \ , \text{and} \quad c = \frac{1}{\tau_t}$$

are constants,

$\tau = r \times C_t$, $\tau_0 = R \times C_0$, and $\tau_t = R \times C_t$,

are the characteristic times of the charge distribution processes.

The general solution to Eq.(9.7) can be written in a form:

$$v(t) = A \times \exp(x_1 \times t) + B \times \exp(x_2 \times t) \ , \qquad (9.8)$$

where *A* and *B* are constants and $x_{1,2}$ are solutions of the relevant characteristic equation:

$$x_{1,2} = \frac{-b \pm \sqrt{b^2 - 4ac}}{2a} \ , \qquad (9.8a)$$

Constants *A* and *B* can be found from the initial conditions:

$$v(0) = 0 \quad \text{and} \quad \left.\frac{dv}{dt}\right|_0 = \frac{U_0}{r \times C_0} \, , \qquad (9.9)$$

from where

$A + B = 0$, and

$$A \times x_1 + B \times x_2 = \frac{U_0}{r \times C_0} \ .$$

Finally, constants *A* and *B* can be expressed as follows:

$$A = \frac{U_0}{r \times C_0 \times (x_1 - x_2)}, \ B = -A \, , \qquad (9.10)$$

Note that at $b_2 >> 4ac$, $x_1 = -1/(\tau + \tau_0 + \tau_t)$, or considering that $\tau << \tau_0 + \tau_t$, the decreasing part of the $v(t)$ function can be approximated as

$$A \times exp(-t/R(C_0+C_t)). \quad (9.11)$$

To evaluate how variations of different parameters of the model affect absorption voltages, let us consider a 1 μF capacitor that has been precharged for a long time, so U_0 = 10 V, briefly discharged, and then V_{abs} is monitored with time using a voltmeter with an internal resistance that exceeds substantially the resistance associated with the leakage current. Assuming that the resistance of the relaxator r = 100 Mohm, and the leakage resistance R = 10 Gohm, the effect of variation of the absorption capacitance, C_t in the range from $0.1 \times C_0$ to $3 \times C_0$ is shown in Figure 9.1.a. As expected, the amplitude of V_{abs} increases with C_t; however, the increase is sublinear, and at $r << R$ can be approximated with a simple function that is derived based on charge redistribution from C_t to $(C_t + C_0)$: $V_{max} = U_0 \times C_t/(C_t + C_0)$.

The effect of the resistance of the relaxator, r, for a 1 μF 10 V capacitor having R =1 Tohm and C_t = 0.5 μF is shown in Figure 9.1.b. Increasing r from 100 Mohm to 1 Tohm affects mostly the time of the voltage onset, whereas the decreasing portion of the curve remains practically unchanged. As it was discussed before, an increase of r to the level of R results in decreasing of the maximum voltage, so relaxators with $r >> R$ do not affect absorption voltages.

Assuming that for the capacitor that is considered above the resistance of the relaxator is constant, r = 10 Gohm, but the insulation resistance, R, varies from 1 Gohm to 10 Tohm, kinetics of variations of absorption voltages is shown in Figure 9.2.c. At R exceeding r the amplitude of V_{abs} remains constant, but the time to the roll-off increases with R substantially.

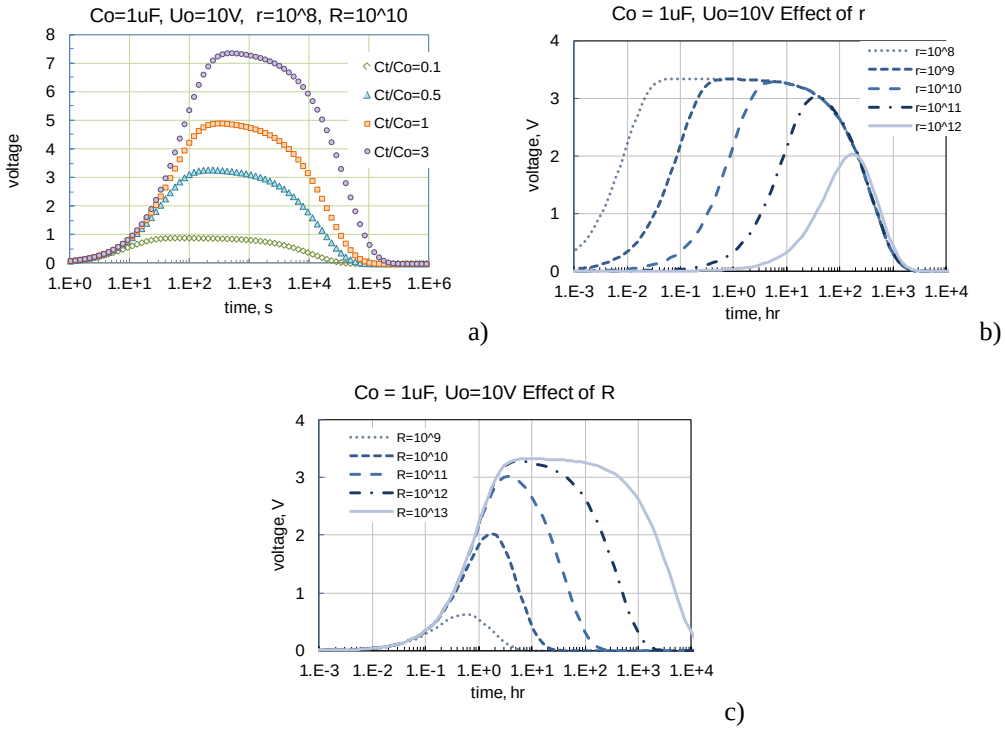

Figure 9.2. Simulation of absorption voltages in a 1 μF 10 V capacotor having different absorption capacitances, C_t, at $r = 10^8$ ohm and $R = 10^{10}$ ohm (a), different values of the relaxator resistance, r, at C_t

= 0.5 μF and $R = 10^{12}$ ohm (b), and different insulation resistances, R, at $r = 10^{10}$ ohm and C_t = 0.5 μF (c).

Variations of V_{abs} for a 4.7 μF capacitor with time after charging to 16 V were calculated per Eq. (9.8) at values of the relaxator resistance $r = 10^{10}$ Ohm, insulation resistance R = 10^{11} ohm, and values of C_t ranging from 0.03 μF to 10 μF. Results of these calculations are shown in Figure 9.3. The amplitude of V_{abs} increases with C_t and can be roughly estimated as $V_{abs\text{-}max} = U_0 \times C_t /(C_t + C_0)$. The rate of decreas can be estimated as a slope in log-linear coordinates and is equal to 2.92×10^{-3} for C_t = 10 μF, 5E-3 for C_t = 3 μF, and 6.65×10^{-3} for C_t = 1 μF and lesss. These values can be estimated as predicted per Eq.(9.11).

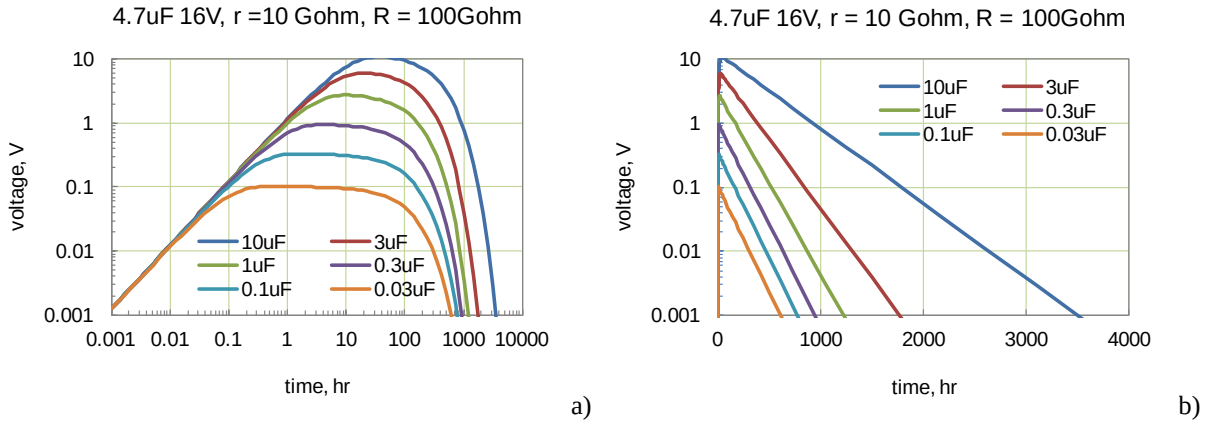

a) b)

Figure 9.3. Simulations of absorption voltages in a 4.7 μF capacitor having $r = 10^{10}$ ohm and $R = 10^{11}$ ohm at different values of C_t in double logarithmic (a) and log-linear coordinates (b).

Westerlund and Ekstam [22] analyzed absorption processes in capacitors that follow Curie van Schwendler law and got analytical solutions for $V_{abs}(t)$ for a capacitor that have been precharged for some time and then left disconnected. In an assumption that the capacitor has no leakage currents, application of a step voltage U_0 results in currents that can be presented in the form similar to Eq.(1.2):

$$i(t) = \frac{U_0}{h \times t^n} \quad , \qquad (9.12)$$

where n and h are constants, and $0 < n < 1$

Laplace transformation of this current is

$$I(s) = \frac{\Gamma(1-n) \times U_0}{h \times s^{1-n}} \quad ,$$

where s is the Laplace parameter (complex frequency, iω), and

$\Gamma(n) = \int_0^\infty e^{-t} t^{n-1} dt$ is the gamma function.

If voltage across the capacitor is changing with time, $u(t)$, the relevant current variation and its Laplace image can be written in the form:

$$i(t) = \frac{\Gamma(1-n)}{h}\frac{d^n u(t)}{dt^n} \quad \text{and} \quad I(s) = \frac{\Gamma(1-n)}{h}s^n U(s)$$

For a situation when a capacitor was charged from a power supply for a period of time from $t = -T$ to $t = 0$ and then at $t > 0$ left disconnected, the charging and discharging currents through the capacitor can be written as:

$$i_c(t) = \frac{U_0}{h \times (T+t)^n} \quad \text{and} \quad i_d(t) = \frac{\Gamma(1-n)}{h}\frac{d^n u(t)}{dt^n},$$

where $T + t > 0$, and $t > 0$

The open circuit condition means that the charge current at voltages $u(t)$ is compensated by the discharge current. This balance of currents can be written as a function of the absorption voltage.

$i_c(t) + i_d(t) = 0$, or:

$$\frac{U_0}{h \times (T+t)^n} + \frac{\Gamma(1-n)}{h}\frac{d^n u(t)}{dt^n} = 0 \tag{9.13}$$

A solution to this differential equation is:

$$u(t) = \frac{U_0}{\Gamma(1-n)\Gamma(n)}\int_0^T \frac{d\tau}{\tau^n (T+t-\tau)^{1-n}} \tag{9.14}$$

Considering that $\Gamma(z)\Gamma(1-z) = \frac{\pi}{\sin(\pi z)}$, the above equation can be simplified:

$$u(t) = U_0 \frac{\sin(n\pi)}{\pi}\int_0^T \frac{d\tau}{\tau^n (T+t-\tau)^{1-n}} \tag{9.15}$$

At $t << T$, $u(t) \sim U_o$, and at $t >> T$ we can neglect values of T and τ, so $(T+t-\tau)^{1-n} \sim t^{1-n}$ and

$$u(t) \approx U_0 \frac{\sin(n\pi)}{\pi}\left(\frac{T}{t}\right)^{1-n}$$

This means that the absorption voltage is a function of n and the precharge time T only, and at n close to 1 V_{abs} in a capacitor with negligible leakage currents will decrease slowly, as $\sim t^{n-1}$.

Laplas transformation allows also for calculation of the dielectric constant [1]:

$$\varepsilon' = \varepsilon_\infty + \omega^{n-1} \times \frac{1}{2h} \times \Gamma(1-n) \times \cos\left(\frac{1-n}{2}\pi\right)$$

At n slightly below 1 the dielectric constant, and hence the capacitance, will slowly grow as frequency decreases from the hertz to milli- and micro-hertz range as $C \sim f^{n-1}$, $0 < n < 1$. This can explain the difference between capacitance values calculated based on measurements of *I-t* characteristics during constant voltage measurements and *V-t* characteristics during constant current measurements (see section VII). In the first case, the time range (up to 10 ksec) is close to the micro-hertz frequencies, while in the second case (up to dozens of seconds) – to milli-hertz frequencies.

X. Absorption voltages in virgin and fractured capacitors

Examples of absorption voltages measured with time after 1-hour polarization at rated voltages followed by a 5-second short circuit are shown in Figure 10.1. This procedure, polarization at VR for one hour followed by a 5-sec short-circuit period, is a default process for V_{abs} measurements used in our experiments. Results in Figure 10.1 show a high reproducibility of the measurements from sample to sample. The voltage increases with time during a period that for different part types varies from several hours to several dozens of hours and then decreases gradually with time. In most cases the maximum V_{abs} exceeded 1 or 2 volts, and the capacitor remains at voltages more than 1 V even after hundreds of hours of storage at room conditions. The maximum value of V_{abs} does not correlate with the value of capacitance and in some cases absorption voltages as large as 5 to 8 volts were reached after a few hours of storage for capacitors in the nanofarad range.

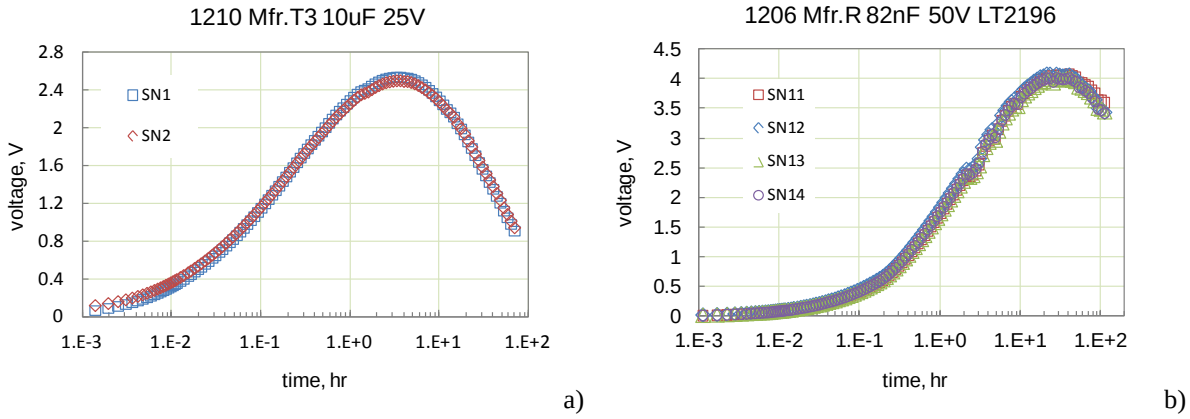

Figure 10.1. Variations of absorption voltages in two samples of 10 µF 25 V (a) and four samples of 82 nF 50 V (b) X7R capacitors.

The presence of a relatively low voltage across the capacitors during storage might initiate degradation processes similar to those that cause failures in capacitors with defects during low-voltage humidity testing. Several cases of failures in ceramic capacitors after long-term storage have been reported. Holladay [23] observed failures in a group of 100 capacitors stored on the shelf for 2 years at room ambient. These parts had IR ~15 kohm at 2V, but the value jumped to ~300 Mohm at 16V, which is typical for the low-voltage failure phenomenon. Three out of 30 virgin CDR31BP470BJMS capacitors from a lot suspected to be defective and causing failures in hybrids were found "leaky" during initial testing [24]. Assuming that initially all these MIL-spec parts were normal, the observed 10% failures can be ascribed as a storage-induced failures. Several cases of failures in MLCCs were observed during unbiased testing at 85 °C/85% RH. It is possible that although capacitors were not biased, absorption voltages have created conditions similar to low-voltage humidity testing.

An increase in duration of the polarization period enlarges V_{abs} (see Figure 10.2) and so does an increase in the voltage during polarization (see Figure 10.3). In all cases there was a trend for saturation of absorption voltages at high levels of polarization.

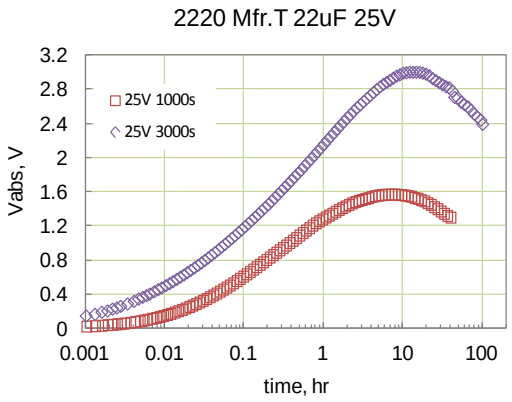

Figure 10.2. Kinetics of V_{abs} variations in 22 µF 25 V capacitors after polarization at 25 V for 1000 sec and 3000 sec.

Time dependence of the absorption voltage is in agreement with the model described in section IX. Initially, the voltage increases due to discharge of capacitors C_t onto C_0 and after reaching maximum decreases due to charge leaking through the insulation resistor R (see Figure 9.1). Dashed lines in the V_{abs} charts shown below are calculations per Eq.(9.8) using the best-fit approximation and parameters'ajustment technique. The values of C_t used for calculations were obtained from *I-t* characteristics as discussed in section VII. Results of calculations of the insulation resistance based on voltage absorption measurements, IR_{abs}, are shown in Table 10.1.

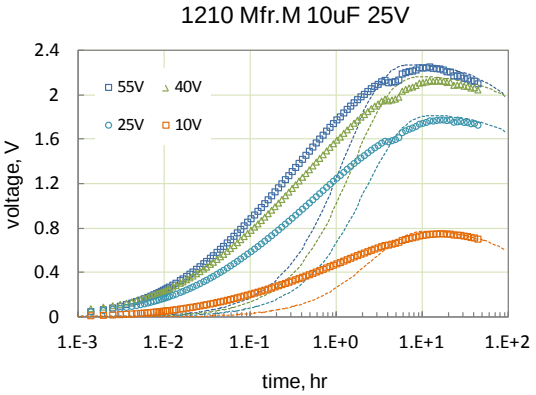

a)

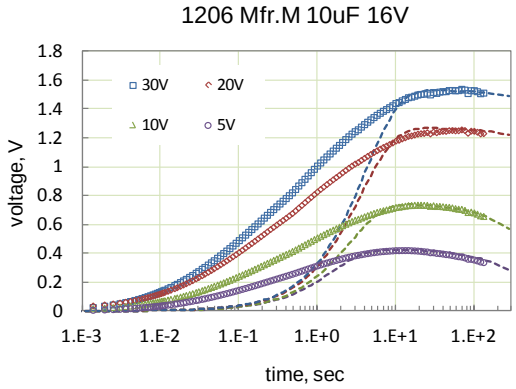

b)

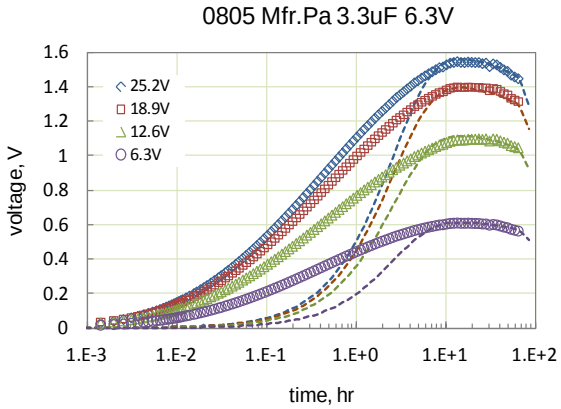

c)

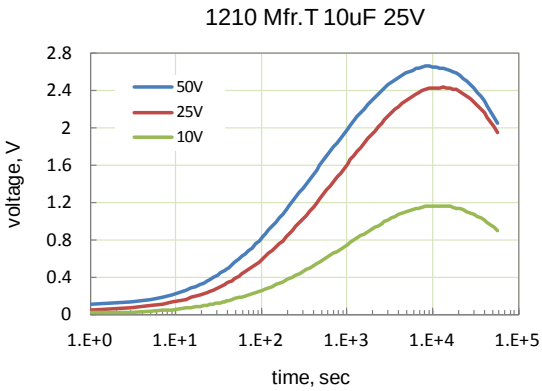

d)

Figure 10.3. Effect of polarization voltage on absorption voltages in different types of X7R capacitors.

To assess how environmental conditions affect absorption voltages, 1 μF 50 V capacitors were measured first at room conditions, and second time the part after polarization and short circuit was installed in a humidity chamber at room temperature and 98% RH. In the latter case the IR value was expected to drop substantially due to increased surface conductivity of ceramic in humid environmernts. Results of these tests are shown in Figure 10.4. In the first case, the voltage increased gradually and reached ~ 4.5 V after approximately 100 hours, and then slightly dropped (to ~ 4.4 V) after ~ 300 hours of storage. Calculations showed that IR of the part in normal conditions was ~ 10^{13} Ohm. In high humidity, the voltage increased to ~0.92 V after ~ 0.1 hr and then decreased to below 50 mV after 0.3 hr and remained low up to 18 hours. In this case calculations resulted in a resistance approximately five orders of magnitude less, IR ~ 2×10^{8} Ohm. After 18 hours of discharging in the humidity chamber the part was removed and the following measurements were carried out at room conditions (22 °C and 50%RH). Reduction of IR due to desorption of the excessive moisture resulted in a gradual increase in absorption voltage up to ~ 2 V after 200 hours, affter which the test was terminated. These data show that even prolonged short circuit conditions (up to ~ 20 hours) are not sufficient to fully discharge capacitors, and substantial voltage increase can occur even after hundreds of hours of storage.

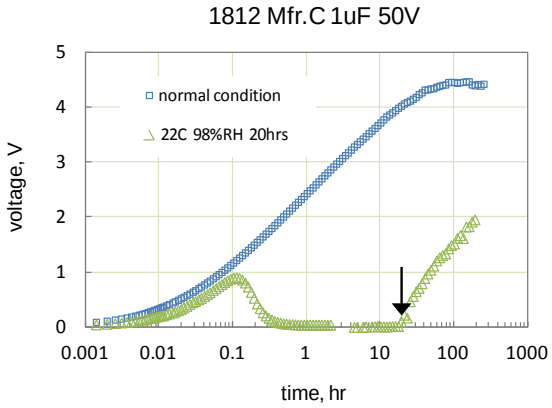

Figure 10.4. Absorption voltages in a 1 μF 50V X7R capacitor measured at room conditions (22 °C and 50%RH) and in high humidity (22 °C and 98%RH). An arrow indicates a moment (~ 20 hours) when the capacitor was removed from the humidity chamber.

Figure 10.5 shows results of V_{abs} measurements in 0.1 μF 50 V COG capacitors. The absorption voltage increased almost linearly in the range of polarization voltages from 25 V to 75 V, but the maximum voltage was relatively low, below 0.4 V, and it was reached relatively fast, after 20 to 30 hours. Based on calculations at different voltages, the value of resistance was ~ 5×10^{13} Ohm. A relatively low value of the maximum voltage is likely due to a low capacitance of traps, C_t ~ $0.03\times C_0$, that was determined based on I-t measurements (see Figure 7.3.)

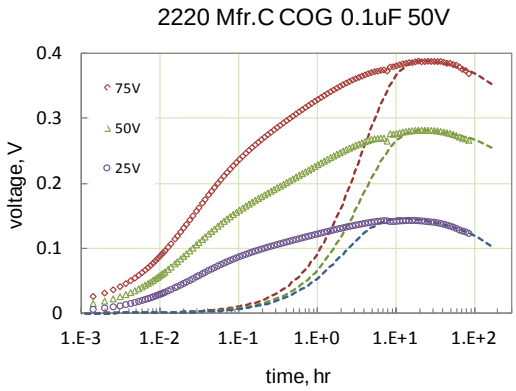

Figure 10.5. Absorption voltages in COG 0.1 µF 50 V capacitors.

Comparison of absorption voltages in different types of X7R capacitors in normal condition and after cracking introduced by the Vickers inductor is shown in Figure 10.6. In the damaged capacitors a decrease of V_{abs} occurs much earlier and the reproducibility of test results is much worse compared to normal parts, which is obviously due to uncontrollable level of damage to the parts.

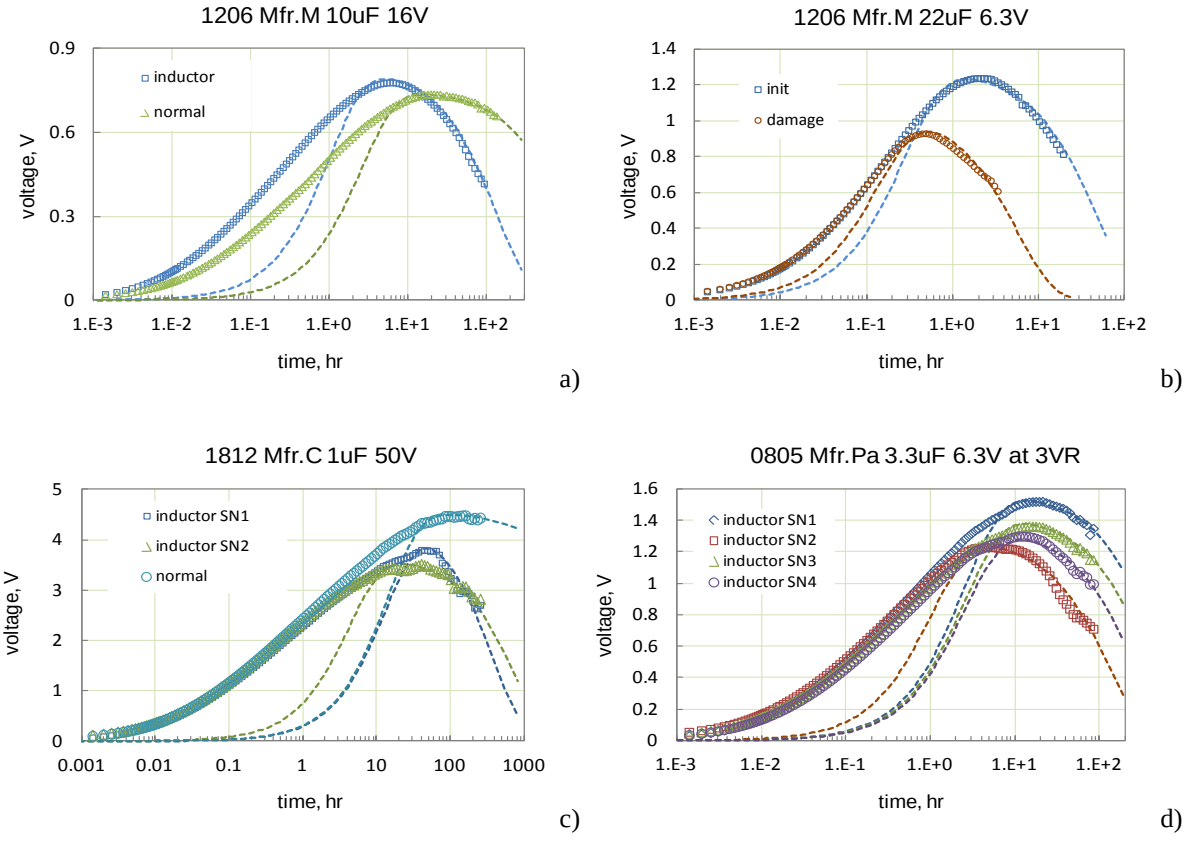

Figure 10.6. Absorption voltages in normal and damaged by the Vickers inductor ceramic capacitors.

Two types of thermal shock, ice water test and solder dip test, were used to evaluate the effect of cracking on absorption voltages in large-size (EIA 2220) 10 µF 50 V and 1 µF 50 V capacitors. Results of these tests are shown in Figure 10.7. For 10 µF capacitors the initial value of IR was ~10^{13} ohm and

it reduced to ~1.5×10^{10} ohm after fracturing. For 1 µF capacitors the difference was less dramatic, but still IR decreases an order of magnitude, from 3×10^{12} ohm to 3×10^{11} ohm.

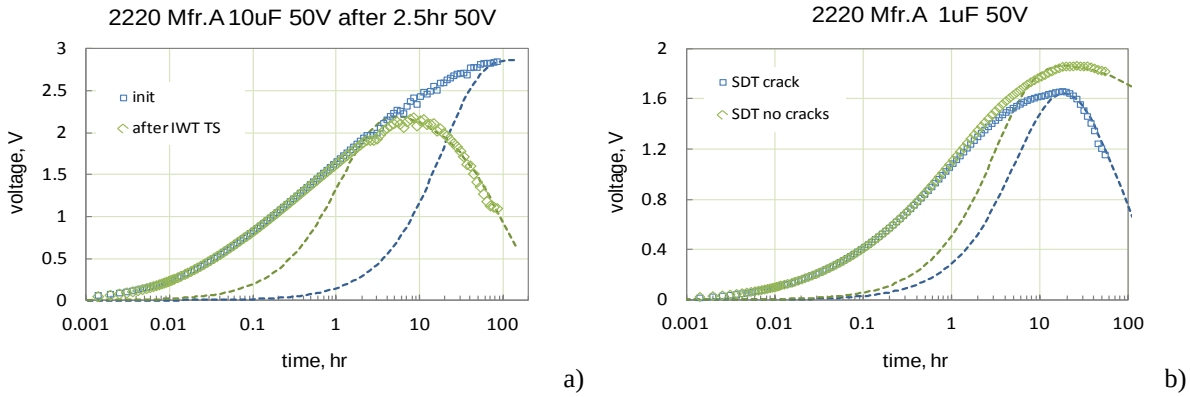

Figure 10.7. Effect of the ice water thermal shock (a) and solder dip thermal shock (b) on 1 µF 50 V X7R capacitors from manufacturer C.

The effect of mechanical fracturing on absorption voltages in several types of X7R MLCCs is shown in Figure 10.8. In all cases the roll-off of V_{abs} starts much earlier in fractured capacitors compared to parts in the normal condition (minutes and hours for damaged parts compared to dozens and hundreds of hours for normal capacitors). For 1 µF 50V capacitors in case size 1825 (Figure 10.8.a) calculations showed that in normal conditions IR values exceeded 3×10^{12} ohm, but for fractured capacitors they were substantially less, 5×10^{11} ohm for SN1 and 5×10^{10} ohm for SN2. For capacitors shown in Figure 10.8.b fracturing reduced resistance more than four orders of magnitude, from more than 5×10^{13} ohm to 8×10^{8} ohm in SN1 and 2×10^{9} ohm in SN2. A relatively small value capacitors in large packages, 0.1 µF 100V in cases size 1825, IR in normal conditions exceeded 5×10^{14} ohm (see Figure 10.8.c) and decreased after fracturing to 2.5×10^{12} ohm in SN1 and to 7×10^{10} ohm in SN2.

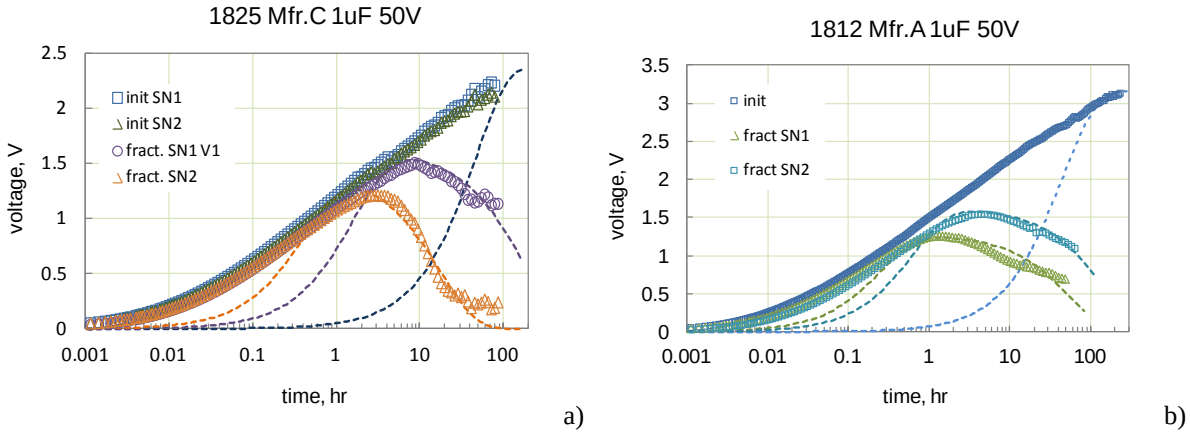

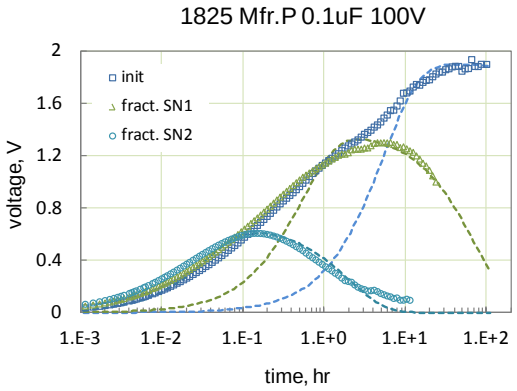

c)

Figure 10.8. Comparison of absorption voltages in normal and mechanically fractured different types X7R capacitors.

In all cases fracturing resulted in noticeable changes in the absorption voltages, and the calculated values of IR_{abs} were substantially less in the damaged capacitors (see Figure 10.9). The resistance in capacitors with cracks remained rather large, typically exceeding 10^9 ohm, which is close to the specified values for high-value commercial ceramic capacitors.

Table 10.1 has also IR values for normal and fractured capacitors calculated based on currents measured after 1 hour of polarization, IR_{1hr}. In all cases, except for four high volumetric efficiency capacitors, currents at rated voltages did not stabilize even after 1 hour of polarization, so the measured current was due to absorption processes and only estimations of minimal values of IR could be made. For the four high-volumetric efficiency parts the values of IR calculated based on current measurements were 10 to 100 times greater than resistances calculated based on measurements of absorption voltages. This difference is most likely due to super-linear variations of leakage currents, and hence, decreasing resistances with voltage. Currents for the IR_{1hr} calculations were measured at rated voltages, whereas Vabs did not exceed a few volts. Respectively, much lower resistances are expected in the first case.

Table 10.1. Insulation resistance in normal and damaged capacitors calculated based on measurements of absorption voltages and direct measurements of currents after 1 hour of poling.

#	EIA size	Mfr.	Co, uF	VR, V	Diel.	Ct/C0	IR_{abs_norm}, Ohm	$IR_{abs\_damaged}$, Ohm	IR_{1hr_norm}, Ohm	$IR1hr_{damaged}$, Ohm
1	0805	N	0.1	50	X7R	0.07	5.0E+12		>1e12	
2	0805	Pa	3.3	6.3	X7R	0.4	5.0E+11	1e11 to 4e11	>1e10	>1e10
3	1206	M	10	16	X7R	0.23	2-3E12	4.0E+10	2.0E+10	6.7E-09
4	1206	M	22	6.3	X5R	0.3	6.0E+09	7.0E+08	>1e9	2.0E+07
5	1206	C	4.7	25	X7R	0.23	4.0E+11	2.0E+10	>1.5e10	2.5E+09
6	1206	A	0.47	25	X7R	0.2	3-5e12		>3e11	
7	1206	R	0.082	50	X7R	0.34	2.5E+12			
8	1210	M	10	25	X7R	0.13	3.0E+11	2.5E+11	1.0E+09	2.0E+08
9	1210	T3	10	25	X7R	1.7	6.0E+09	5.0E+09	5.0E+08	5E+08
10	1210	T	10	25	X7R	1.4	6.0E+09	6.0E+09	5.0E+08	
11	1210	A	0.1	50	X7R	0.4	3.0E+13	2.0E+13	>2e11	>2e11
12	1812	A	1	50	X7R	0.3	5.0E+13	1.5E+09	>5e10	5.0E+08
13	1812	C	1	50	X7R	0.35	3.0E+13	1.5E+12	>3e10	>3e10

14	1825	C	1	50	X7R	0.25	>3e12	5.0E+10	>1e11	2.5E+10
15	1825	P	0.1	100	X7R	0.07	>1E14	2e10 to 3e11	>1e13	2.0E+10
16	2220	T	22	25	X7R	0.136	5.0E+10		>2.5e9	
17	2220	A	1	50	X7R	0.13	3.0E+12	3.0E+11	>1e11	>1e11
18	2220	A	10	50	X7R	0.3	1.0E+13	1.5E+10	>1e10	5.0E+09
19	2223	C	0.022	50	COG	0.5	1.0E+14		>1e12	
20	2220	C	0.1	50	COG	0.28	5.0E+13		>1e13	

Even after 1 hour of polarization absorption currents were prevailing in 80% of cases, so only conservative estimations of the intrinsic IR could be made. Measurements of absorption currents allowed for assessments of IR for normal capacitors in 90% of tested parts. Figure 10.9.a shows correlation between IR_{abs} values for normal and fractured capacitors. In ~ 25% cases fracturing practically did not change IR, but in most cases it resulted in a substantial decrease of IR up four orders of magnitude.

Correlation between IR calculated based on current and absorption voltage measurements for capacitors with cracks is shown in Figure 10.9.b. For these parts, on average, IR_{1hr} values were about an order of magnitude lower than IR_{abs}. As previously, this can be explained by the difference in effective measurement voltages used in the two techniques.

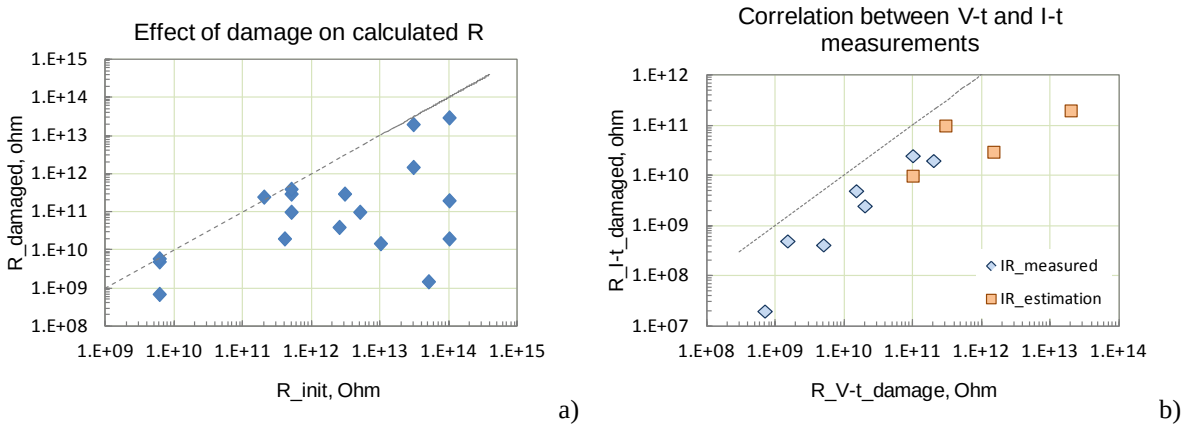

Figure 10.9. Effect of fracturing on the value of resistance calculated based on absorption voltage measurements, R_{abs}, (a) and correlation between R_{abs} and IR calculated based 1-hour leakage current in fractured MLCCs (b). The estimated values of IR_{1hr} in Figure b) are based on measurements of non-stabilized currents after 1 hour of polarization.

Figure 10.10 shows correlation between the resistances IR_{abs} and capacitances for normal and damaged MLCCs. In spite of the large spreading of data, there is a clear trend of decreasing resistance with capacitance. More than that, the dependence of IR_{abs} on C_0 is close to inversely proportional that is expected because a resistance of a dielectric is proportional to its thickness, d, and inversely proportional to the surface area, S, whereas capacitance is proportional to S and inversely proportional to d. The trend of IR_{abs} decreasing with C_0 for capacitors with cracks is not quite clear, but might be partially explained assuming that cracks of the same size would cross a larger number of dielectric layers in parts with thinner layers, and hence have lower resistance.

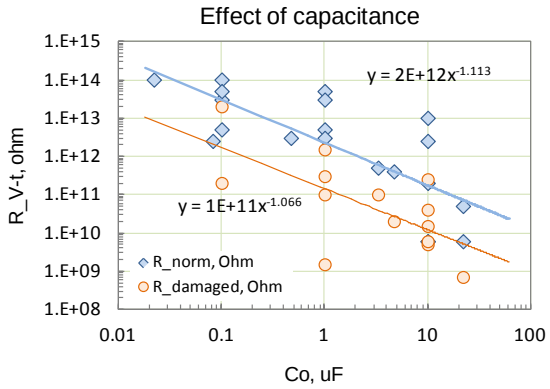

Figure 10.10. Effect of capacitance on resistance calculated based on absorption voltage measurements calculated for normal capacitors and capacitors with cracks.

XI. Discussion

Results of this study show that absorption currents are dominating for MLCCs in the time range that is used for IR measurements, up to 120 sec. Figure 11.1 shows typical current relaxations in large-value MLCCs, from 1 μF to 100 μF. Three areas are observed on the *I-t* curves: charging currents, I_{ch}, that might prevail at times below ~ 1 sec, absorption currents, I_{abs}, prevailing at times below a few hours, and leakage currents that might be observed at times exceeding a few hours. The latter is a sum of the intrinsic leakage current, I_{il}, that is caused by conduction through the bulk of the dielectric layers, and defect-related leakage current, I_{dl}, that is caused by structural or mechanical defects like cracks and delaminations. In a general case, a current through a capacitor under step voltage V can be presented as:

$$I(t,T,V) = I_{ch}(t,V) + I_{abs}(t,T,V) + I_{il}(T,V) + I_{dl}(T,V,RH) \quad (11.1)$$

We are considering relatively short periods of time (minutes to hours) that might be used for IR measurements, so possible long-term degradation similar to one shown in Figure 4.6 that can change leakage currents with time under stress is assumed negligible, and I_{il} and I_{dl} are time independent. All components in the equation above depend on the external factors including voltage and temperature and these dependencies will be analyzed below. Charging currents depend on the applied voltage and external resistance only as described in Eq.(1.1) and after a few seconds of electrification do not affect IR measurements. The component of leakage currents associated with cracks depends also on the relative humidity of environments.

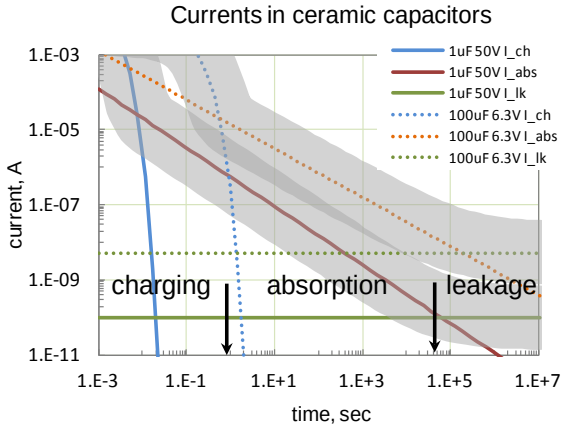

Figure 11.1. Currents in high-value MLCCs after application of rated voltages. Gray area shows a typical range of current variations.

For the quality assurance purposes it is important to assess the defect-related component of the current. To optimize test conditions (voltage and temperature) we need a better understanding how external factors affect different components in Eq.(11.1). Absorption currents and intrinsic leakage currents are greater for larger value capacitors, and for this reason revealing defects in high volumetric efficiency commercial capacitors might be a challenge.

- *Absorption currents.*

Our data show that absorption currents dominate during standard IR measurements, and the leakage currents can be revealed after hours of polarization only. At relatively low voltages, typically below 2-3 times VR, I_{abs} increases with voltage linearly and practically does not depend on temperature. Short circuit (depolarization) currents flow in the opposite direction but have the same isochronic values as polarization currents. These facts that are consistent with literature data [1, 25] can be explained assuming that the absorption process is due to phonon-assisted tunneling of electrons from electrodes into states (traps) located in the forbidden energy gap of the dielectric at the interface with metal electrodes. Different energy levels of these traps change the probability of trapping and due to exponential dependence on the barrier height can explain substantial variations of the characteristic times for different relaxators used in the Dow model. Different distributions of the trap density with energy might result in different distribution of characteristics times causing variations of the exponent in the Curie van-Schvendler law, Eq.(1.2) as it was shown in section VIII.

A close location of the traps to the electrodes (likely within dozens of angstroms), results in most of the trapped charges flowing back to the electrodes under shorting conditions and in the reversibility of the absorption process. Charges that are trapped within the bulk of the dielectric will be emptied towards both electrodes resulting in a negligible current in the external circuit. A saturation of absorption currents at high voltages that was observed in several cases is due to filling up of the traps and can be used to assess their concentration.

The concentration of traps, N_t, can be calculated based on measurements of the absorption capacitance, C_t. As it was shown in section IV, the value of C_t that is determined at voltages close to the rated, VR,

is proportional to the value of the nominal capacitance, $C_t = \alpha \times C_0$, where α is a constant that for most cases is ~0.3. In this case:

$$C_t = \frac{q \times N_t \times S}{VR} = \alpha \frac{\varepsilon \times \varepsilon_0 \times S}{d}, \qquad (11.2)$$

where d is the thickness of the dielectric, S is the surface area of electrodes, ε is the dielectric constant of the dielectric, $q = 1.6 \times 10^{-19}$ C is the electron's charge, and $\varepsilon_0 = 8.89 \times 10^{-14}$ F/cm is the dielectric constant of vacuum. From (11.2) the value of N_t can be calculated as:

$$N_t = \alpha \frac{\varepsilon \times \varepsilon_0 \times VR}{d \times q}. \qquad (11.3)$$

Assuming for a typical X7R capacitor VR is in the range from 6 V to 50 V, d from 5 μm to 15 μm, and $\varepsilon = 3000$, N_t is in the range from 6×10^{12} cm^{-2} to 2×10^{13} cm^{-2}, which is reasonable considering that the surface concentration of atoms is ~10^{15} cm^2.

Donor-like traps in ceramic capacitors are often associated with the presence of oxygen vacancies. These vacancies are positively charged and their redistribution during HALT results in the reduction of IR and is considered a mechanism of failures specific to BME capacitors. If electron traps that are responsible for absorption currents are associated with oxygen vacancies then we can expect an increase of their concentration at the surface of cathode as a result of HALT. To verify this model, 1 μF 50 V capacitors from three manufacturers were tested at 182 °C 200 V for 100 hours. This testing resulted in about an order of magnitude increase in leakage currents in two out of three part types (see Figure 11.2.a). Annealing at 182 °C reduced currents several times indicating that the oxygen vacancies-related degradation most likely is the reason for variations of leakage currents observed in parts from Mfr.C and Mfr.M. However, absorption currents did not change in the process of annealing (see Figure 11.2.c and d), so absorption processes are likely not related to degradation of IR during HALT.

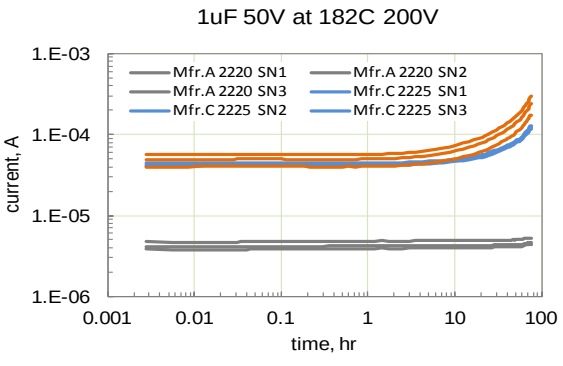

a)

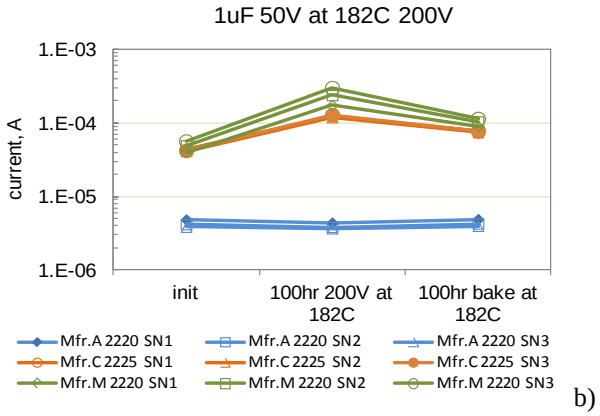

b)

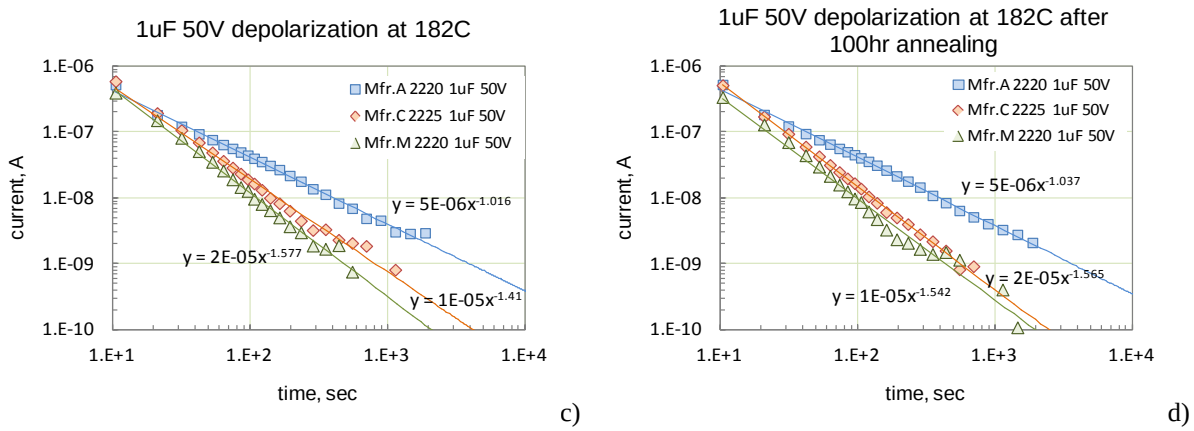

Figure 11.2. Results of highly accelerated life testing, HALT, at 182 °C 200 V (a) and post-HALT annealing at 182 °C (b) for 1 μF 50V capacitors from three manufacturers. Figures c) and d) show depolarization currents measured at 182 °C after poling at 50 V for 5 min initially (c) and after 100 hours of annealing (d).

It is possible that relatively deep electron states involved in absorption processes are spread evenly through the dielectric, but only traps that are located within tunneling distance to the electrodes are responsible for the observed currents. Assuming that the tunneling distance is $l \sim 1$ nm to 3 nm, the volumetric concentration of traps can be calculated as $n_t = N_t/l$ is in the range from 2×10^{21} cm^{-3} to 2×10^{22} cm^{-3}, which might be reasonable for polycrystalline ceramics.

As it was shown in section VI, capacitors with mechanical defects in some cases had greater absorption currents compared to undamaged capacitors. It appears as if mechanical damage increases trap concentration in the dielectric, which is difficult to comprehend considering that mechanical damage creates local defects, so even at increased concentration of traps in the damaged area, their total effect on absorption processes should be relatively small. To get a better understanding of the problem, several 10 μF 25 V and 10 μF 16 V capacitors from different manufacturers were hit with an instrument that was used to cause inductor-induced damage to simulate mechanical shock conditions, but without fracturing the parts. Variations of capacitances and dissipation factors measured at 1 kHz with the number of hits and with time after the hit are shown in Figure 11.3.

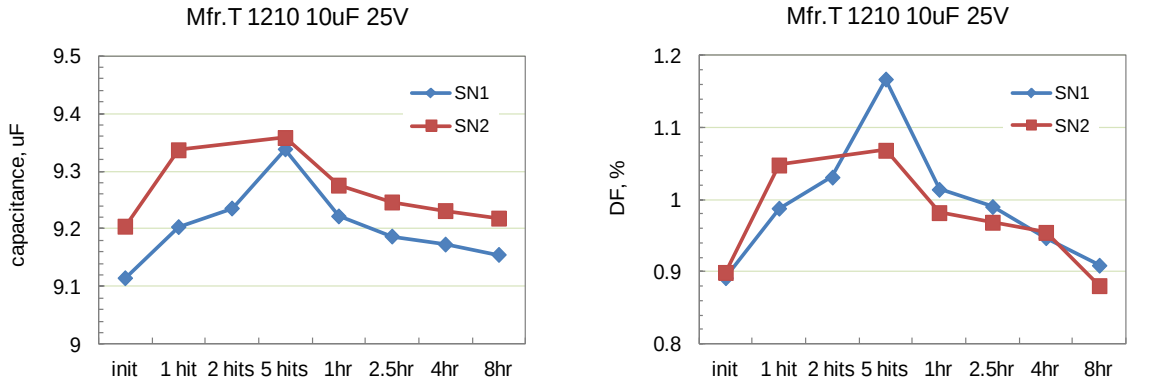

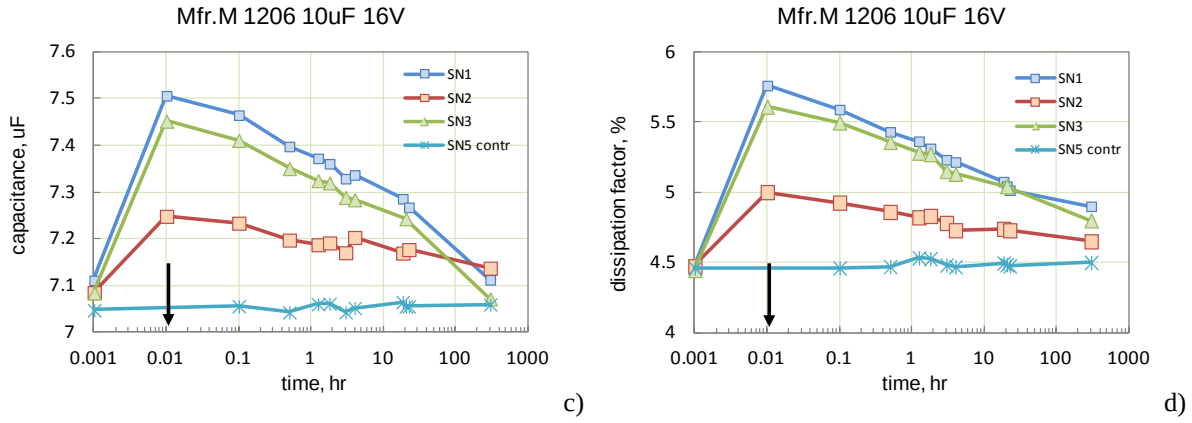

Figure 11.3. Variations of capacitance (a, c) and dissipation factor (b, d) measured at 1 kHz for 1210 10 μF 25 V (a, b) and 1206 10 μF 16 V (c, d) capacitors during the hit simulation testing. Arrows indicate the moment of hitting.

Hitting increases capacitance on 2% to 7% and DF on 20% to 30%, but this increase is reversible: both characteristics gradually decrease with time and after dozens and hundreds of hours tend to stabilize at the initial level. A decrease of AC characteristics occurs apparently linearly with logarithm of time.

This phenomenon is most likely related to the ageing processes that are due to gradual changes in the domain structure of the dielectric as a result of stress relaxation. It is possible that mechanical stresses associated with the acoustic wave that is formed during hitting disturb the domain structure that then relaxes with time of storage. Although more analysis and experiments are necessary to get a better understanding of this phenomenon, it is quite possible that the observed increase in the absorption currents in damaged capacitors is due not to the cracking, but rather to generation of traps caused by a mechanical shock associated with fracturing.

Results show that mechanical shock can change AC characteristics of X7R capacitors and this effect, similar to the microphonic effect, should be considered for sensitive circuits.

- *Intrinsic leakage currents.*

To analyze leakage currents in MLCCs it is important to make sure that sufficient time is given to reduce absorption currents so the measured currents are true steady-state leakage currents. At room temperature and rated voltages this stabilization might take many hours; however, the time required to reveal I_{il} can be reduced substantially by increasing voltages and temperatures during testing. Contrary to the absorption currents, intrinsic leakage currents increase with voltage superlinearly, so at sufficiently high voltages, typically exceeding VR, these currents are dominating in the total current through a capacitor already after a few seconds of polarization.

Ceramic materials used in MLCCs are good insulators and it has been established that their conduction is related to electrons injected from metal electrodes [13, 26]. However, there is no agreement in literature on the mechanism of electron transport. The mechanism of conduction through ferroelectric materials was attributed to the electrode-limited Schottky emission [27-29], bulk-limited Poole-Frenkel transport [30-31], or space charge limited, SCL, conduction [25, 32].

Schottky injection is the most commonly observed currents in ferroelectric materials [26]. According to the Schottky theory, the electron flow from the metal to the insulator is limited by a surface energy barrier, Φ_B, that changes with applied voltage, so the current density corresponding to this flow, J, is an exponential function of the electric field in the dielectric, E:

$$J_{Sch} = C_{RD} T^2 \exp\left(-\frac{\Phi_B}{kT}\right)\exp\left(\frac{\beta_s E^{0.5}}{kT}\right) \qquad (11.4)$$

$$\beta_s = \left(\frac{q^3}{4\pi\varepsilon\varepsilon_0}\right)$$

where C_{RD} =1.2×10^6 A/m^2_K^2 is the Richardson-Dushman constant, q is the charge of electron, k is the Boltzmann constant, T is the absolute temperature, β_s is the Schottky constant, ε_0 is the permittivity of the free space, and ε ~5.5 is the high-frequency dielectric constant for ferroelectric ceramics [26].

This equation can accurately predict field emission in metal-vacuum systems, but its application to metal-dielectric systems results in anomalously high currents. To resolve this problem Aris [8] suggested the presence of not only a surface barrier in the dielectric, but also a barrier at the surface of the cathode material. The applied field does not affect substantially the cathode barrier, but influences the metal-dielectric barrier and causes current variations as predicted by Eq.(11.4). To penetrate to the dielectric, electrons have to tunnel through the cathode barrier, so their flow to the dielectric is reduced drastically. In this case Eq.(11.4) can be used to describe metal-dielectric systems, but instead of the Richardson-Dushman constant, an empirical parameter should be used.

Another correction of the Schottky model had been made by Simmons [33]. Schottky equation is applicable to the systems with the mean free path of electrons greater than the thickness of the dielectric, which is not valid for MLCCs. It has been shown [26] that for ferroelectric thin films the corrected form suggested by Simmons provides a better agreement with experimental data. According to Simmons, for insulators having small electronic mean free path a modified equation can be written as:

$$J_S = AT^{3/2}\mu E \exp\left(-\frac{\Phi_B}{kT}\right)\exp\left(\frac{\beta_s E^{0.5}}{kT}\right), \qquad (11.5)$$

where A = 3.08E-4 A/cm^2_K$^{1.5}$ is the constant, and μ is the electron mobility in the insulator.

Note, that electrical field E has different meaning in the pre-exponential term, μE, and in the exponent, $\exp(\beta_s E^{0.5})$ [28]. The first, reflects bulk drift velocity of electrons, and an average electric field, V/d, in the bulk of a dielectric can be used for estimation of E. The second factor reflects the barrier lowering and in this case, E is the electric field at the cathode surface that can vary depending on the amount and sign of charges at the interface.

Poole-Frenkel (PF) conduction is due to electrons released to a conduction band from traps in the bulk of the dielectric that similarly to the Schottky model is enhanced by the electric field that reduces the barrier height and increases the probability of detrapping. The current density can be presented in a form similar to Eq.(11.5):

$$J_{PF} = K_t E \exp\left(-\frac{U_t}{kT}\right)\exp\left(\frac{\beta_{PF} E^{0.5}}{kT}\right), \quad (11.6)$$

where K_t is a constant related to trap density, U_t is the energy level of traps below the conduction band, and

$\beta_{PF} = \left(\frac{q^3}{\pi\varepsilon\varepsilon_0}\right)$ is the PF constant that is two times greater than β_S.

According to the space charge limited current, SCLC, model, excessive electrons injected into a dielectric are either drifting in the conduction band or trapped on states in the forbidden energy gap of the dielectric, and both create space charges that affect the electrical field and conduction. The characteristic feature of the SCLC for a system with planar electrodes is quadratic relationship between current and voltage [34]:

$$J_{SLC} = \frac{9}{8}\vartheta\varepsilon\varepsilon_0\mu\frac{V^2}{d^3}, \quad (11.7.)$$

where θ is the trapping parameter that corresponds to the ratio of the free and trapped charges and increases with temperature exponentially, d is the thickness of the dielectric.

The shape of electrodes affects I-V characteristics and in case of SCL currents injected form a point contact the quadratic law per Eq.(11.7) should be replaced with the 3/2 law, $I \sim V^{3/2}$ [35]. It has been shown by Lee and Burton [13, 25, 36] that this type of I-V characteristics, rather than the quadratic relationship per Eq.(11.7), is applicable to ceramic capacitors.

The mechanism of conduction can change from Schottky to PF depending on electrode materials used and temperature of testing. Experiments showed that noble metals [2] usually form a Schottky contact to barium titanate ceramics and PF mechanism is more likely to prevail at higher temperatures.

Discrimination between the conduction models is often made by plotting I-V characteristics in different coordinates. Linearization of the data in Schottky [*ln(I) vs.* $V^{0.5}$], Poole-Frenkel [*ln(I/V) vs.* $V^{0.5}$], or double logarithmic [*ln(I) vs. ln(V)*] coordinates that allows for best fitting is used as a prove for the model and the slope of the plot allows for the assessment of the parameters of the model. Unfortunately, as was shown in sections IV and V, in all cases analyzed in this work the data could be equally well approximated in either of the plots, so the validity of the conduction mechanism should be assessed by a comparison of the theoretical and experimental parameters of the slope. Results of this analysis for 10 different types of capacitors are shown in Table 11.1.

According to Schottky and PF models, I-V characteristics in the relevant coordinates can be approximated with straight lines:

$\ln(I) \sim a_s V^{0.5}$ and

$\ln(I/V) \sim a_{PF} V^{0.5}$,

where a_s and a_{PF} are the slopes that depend on temperature and thickness of the dielectric only:

$$a_s = \frac{\beta_s}{kTd^{0.5}} \quad \text{and}$$

$$a_{PF} = \frac{\beta_{PF}}{kTd^{0.5}}$$

Note that $a_{PF} = 2a_s$ and for this reason Table 11.1 shows theoretical value of the slope for the Schottky model only, a_s.

Analysis of the results shows that experimental values of the slopes determined for the Schottky model exceed the calculated values on average in 3.65 times. Somewhat better results were obtained for the Poole-Frenkel model where the discrepancy between calculated and experimental slopes was ~ 1.8 times. The Simmons model allowed for a much better agreement with the theory and the average ratio of the experimental and calculated slopes was ~ 0.9.

All models predict Arrhenius-like temperature dependence that can be characterized with activation energy, E_a. The values of E_a calculated at relatively low voltages are shown in Table 11.1 and for different part types vary from 0.55 eV to 1.1 eV, which is lower than the values in the range from 1.2 eV to 1.3 eV reported for X7R capacitors by Lee, Burton, et al. [13, 25].

Table 11.1. Calculated and experimental parameters of the model for intrinsic leakage currents.

#	Part	C, μF	VR, V	d, μm	calc. slope as, $(m/V)^{0.5}$	Voltage range, V	PF slope $(m/V)^{0.5}$	Sch slope $(m/V)^{0.5}$	Power expon., m	E_a, eV
1	Mfr.Pa 0805	3.3	6.3	4.5	0.3	25 - 150	0.99	1.23	5*	
2	Mfr.M 1206	22	6.3	2.5	0.4	9 - 140			2.1*	
						9 - 20	0.57	1.1		
						20 - 140	0.36	0.6		
3	L2L	0.68	6.3	2	0.45	10 - 100			4.3*	
						10 - 30	1.6	2.1		
						30 - 100	0.83	1.1		
4	Mfr.M 1206	22	6.3	2.5	0.4	5 - 30	0.41	1	2 – 1.5**	~0.55
5	Mfr.C 1206	4.7	25	5	0.28	5 - 50	0.72	1.2	2.5 – 1.3**	~0.75
6	Mfr.M 1206	10	16	4	0.32	5 - 50	0.66	1.2	2.9 – 1.4**	~0.95
7	Mfr.A 1206	0.47	25	13	0.18	5 - 50	0.5	1.1	2 - 1.7**	~0.95
8	Mfr.C 2225	1	50	13.9	0.17	5 - 150			~1.5***	~1.1
						5 - 40	0.22	0.8		
						40 - 150	0.09	0.3		
9	Mfr.A 2220	1	50	29	0.12	5 - 150	0.15		~1.5***	~0.88
						5 - 40		0.7		
						40 - 150		0.33		
10	Mfr.M 2220	1	50	19	0.15	5 - 150	0.13			
						5 - 40		0.8	~1.5***	~1.1
						40 - 150		0.34		

Notes: * - room temperature data;
** -larger values correspond to room temperature and smaller to 165 °C;
*** - data in the range of temperatures from 125 °C to 182 °C.

It is interesting to note that with the range of E_a from 0.55 eV to 1.1 eV the leakage-related insulation resistance should decrease as temperature raises from room to 125 °C in 3×10^2 to ~ 10^5 times. However, most specifications, military including, reduce requirements for IR at 125 °C ten times only. Obviously, this is related to the fact that a substantial component of the measured currents is due to absorption processes that have weak temperature dependence.

Equations 11.4 and 11.6 show that for Schottky and PF models E_a is decreasing with applied voltage:

$$E_a = E_0 - \frac{\beta_{S/PF}}{d^{0.5}} V^{0.5}, \qquad (11.8)$$

where E_0 is the barrier height in the absence of voltage, and $\beta_{S/PF}$ is equal to β_S for the Schottky of Simpson models and β_{PF} for the PF model.

Variations of activation energy with voltage calculated per Eq.(11.8) for a case when E_0 = 0.7 eV is shown in Figure 11.4. The range of thicknesses of dielectrics is chosen to match experimental data presented in Figure 5.6. Variations of E_a with voltage observed experimentally for different part types are in the range from 7% to 37%, whereas calculations per Schottky model predict decrease in E_a on 2% to 5% only. PF model predicts somewhat larger variations of E_a, from 4% to 10%, which are still below the experimental data. For large-size 1 μF 50 V capacitors shown in Figure 5.8 the difference between theoretical and experimental data is also significant: calculations predict a decrease in E_a from 10 V to 150 V on 3% to 6%, and experimental variations are ~ 17%. Burton [25] considered a decrease in E_a with voltage as an indication of a grain boundaries related transport.

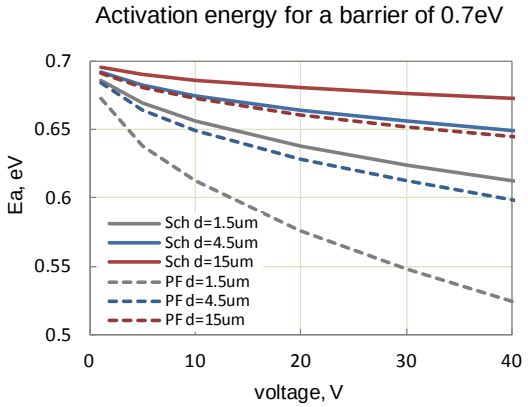

Figure 11.4. Voltage dependence of activation energy calculated per Schottky and Poole-Frenkel models for capacitors with different thickness of the dielectric.

Approximation of I-V characteristics with a power law resulted in the exponent m that at room temperature varied in a wide range, from 2 to 5. However, at high temperatures, from 125 °C to 182 °C three types of large-size 1 μF 50V capacitors from different manufactures had close values of m ~ 1.5. Temperature dependencies of the exponent m shown in Figure 5.4 also indicate that at high temperatures (125 °C and 165 °C) four types of 1206 X7R capacitors had m close to 1.5. This type of I-V

characteristics can be attributed to SCLC in the case of injection from pointed electrodes. Lee et al. [13] and Burton [25] observed the near 3/2 power dependence of currents on voltage for Z5U and X7R capacitors. The results were explained by electron emission from electrode protuberances and asperities that considered a dominant cause of leakage currents in MLCCs. The presence of electrode protuberances in their work was confirmed by cross section and scanning electron microscopy (SEM) that indicated the irregular nature of used electrodes. Deviations from the 3/2 law and I-V curves with the exponent *m* close and greater than 2 were attributed to variations of the parameters of the traps involved in the conduction mechanism.

Our cross-sectional examinations did not reveal substantial irregularities in the electrodes, and considering that the same I-V characteristics were observed for parts from different manufacturers, it appears more likely that the 3/2 law is due to some intrinsic irregularities in the distribution of the electric field caused by the micrograin structure of ceramic materials. Grains that have greater conductivity compared to the shells [26] might play a role of virtual electrodes operating effectively as point contacts for electron injection.

- *Leakage currents caused by mechanical defects.*

Analysis of the external factors affecting damage-related component of the leakage current will be considered in the NEPP report 2013. Based on results presented in this report, leakage currents related to mechanical defects in most cases are below or comparable with the intrinsic leakage currents, so not only standard IR measurements, but even measurements taken after hours of electrification, might not reveal cracks in large value low-voltage ceramic capacitors. Although voltage and temperature dependence of the damage-related leakage currents is not known, this dependence is most likely less strong than for the intrinsic leakage currents. For this reason, attempts to screen-out damaged capacitors by IR measurements at high voltages and/or temperatures are not effective.

- *IR measurements based on absorption voltages.*

Results show that for normal capacitors intrinsic leakage currents at temperatures below 85 °C increase with voltage either exponentially, according to the Simpson equation (11.5), or as a power function with the exponent in the range from 2 to 5. Considering that voltage dependence of the crack-related component of currents is less significant and likely close to linear, to avoid the masking effect by intrinsic leakage currents, it is preferable to measure crack-related component at low voltages. However, leakage currents at low voltages are extremely small and cannot be measured accurately enough. In this regard measurements of absorption voltages that are essentially integrals of the leakage currents and in most cases do not exceed a few volts provide effective means for discrimination of normal and fractured capacitors.

As it has been discussed above, standard measurements of IR that are measured within 1 to 2 min of polarization reflect absorption processes in capacitors and the measured IR in most cases is greater than IR related to intrinsic leakage currents by several orders of magnitude.

In the attempt to get resistance values reflecting leakage currents more closely, IR was calculated based on currents measured after 1 hour of polarization at rated voltages. Results of these measurements, see

Table 10.8, show that in all cases, except for large value capacitors in relatively small case sizes (10 μF 25 V in 1210), only estimations of the minimal IR values could be made. This was due either to the prevailing of absorption currents even after 1-hour polarization or to a low value of leakage current, typically below 10^{-11} A, that was comparable with the accuracy of the test system used. Absorption voltages after roll-off are determined by a charge decrease on the capacitor under test, which is an integral of leakage currents, and thus can provide a more accurate estimation of the IR compared to direct current measurements.

IR values calculated based on V_{abs} were consistent with the IR_{1hr}, but the range of resistance was up to 10^{14} ohm compared to less than 10^{13} ohm for results based on the currents measurements. IR_{1hr} for EIA size 1210 10 μF 25V capacitors were one to two orders of magnitude less than IR_{abs}. This is due to the difference in voltages that was 2 5V in the first case and a few volts in the second case. The one-hour current measurements allowed revealing damage in capacitors in approximately 60% of cases, whereas absorption voltage measurements were successful in 11 out of 14 tested parts (~80%). The only three cases were no decrease in IR_{abs} after damage was observed are the three 1210 10 μF 25 V capacitors that had low IR initially. Obviously, in this case the intrinsic leakage current exceeded damage-related currents and none of the techniques is effective. Excluding cases with high intrinsic leakage currents, the success of IR_{abs} measurements to revel cracks in the parts is close to 100%.

XII. Conclusion

1. Currents in MLCCs after application of a step voltage can be presented as a sum of charging, absorption, and leakage currents. At room temperatures the first component prevails during initial moments, up to ~ 1 sec, the second up to several hours, and the third, that is sensitive to the presence of defects, might be revealed after several hours of polarization.
2. AC characteristics of MLCCs, capacitance and dissipation factor measured at 1 kHz, are not sensitive to the presence of cracks unless the parts are damaged extensively.
3. Insulation resistance that is measured within first 2 minutes of electrification is determined by absorption currents in capacitors that have the following features:
   a. Time dependence of absorption currents in all tested X7R, X5R, and COG capacitors follows Curie von Schweidler power law with the exponent varying from 0.6 to 1.3.
   b. Polarization and depolarization currents are reproducible, have opposite polarity, and their isochronic values are similar.
   c. Absorption currents have a weak dependence on temperature, increase linearly with voltage up to 2 to 3 times VR, and stabilize at larger voltages.
   d. The presence of fine cracks in ceramic capacitors does not affect absorption currents, and hence IR.
   e. Processes of charge absorption in MLCCs can be explained by electron trapping into states at the metal –ceramic interface as a result of tunneling. Absorption capacitance increases with the nominal value of capacitance and is equal on average $0.3\times C_0$ at a standard deviation of 0.16. The concentration of traps is estimated in the range from 6×10^{12} cm^{-2} to 2×10^{13} cm^{-2}.

4. Intrinsic leakage currents in MLCCs increase superlinearly with voltage and exponentially with temperature. Activation energy of leakage currents at low voltages for different types of X7R capacitors is in the range from 0.55eV to 1.1 eV and decreases with voltage.
5. Experimental *I-V* characteristics of intrinsic leakage currents can be linearized equally well in Schottky, Poole-Frenkel, and double logarithmic coordinates that indicates a power dependence of current on voltage. Al low temperatures, the Schottky model with Simmons corrections provides a better agreement between calculated and experimental parameters. At temperatures above 85 °C, *I-V* characteristics follow a power law, $I \sim V^m$, where *m* is a constant close to 1.5. This indicates a space charge limited current, SCLC, mechanism for electrodes of irregular (pointed) shape.
6. Mechanical hits were found to cause increasing of the isochronic absorption currents (in 2 to 5 times) and capacitance measured at 1 kHz. The capacitance increases after hitting on 2% to 7% and dissipation factors on ~25%. These values then decrease to the initial level during hours of storage linearly with the logarithm of time. This phenomenon is similar to the ageing processes in ferroelectric capacitors and most likely is due to a reversible trap generation in the dielectric as a result of hitting.
7. The Dow model was used to explain time dependencies of absorption currents. Variations of the exponent *n* for different types of capacitors are attributed to the specifics of the energy distributions of the density of electron traps that can be modeled by differences in absorption capacitors and characteristic times of *R-C* relaxators employed in the Dow presentation.
8. Analysis of long-term variations of absorption voltages in MLCCs showed the following:
   a. Absorption voltages in MLCCs typically increase within a few hours after polarization at VR, up to several volts. Subsequently, V_{abs} decreases slowly and can remain above one volt even after hundreds of hours. The maximum value of V_{abs} does not correlate with the value of capacitance, increases linearly with polarization voltages below ~3×VR, and stabilizes at greater voltages.
   b. Substantial absorption voltages (more than 2 V) might appear even after prolonged (~20 hours) short circuit conditions.
   c. The maximum value of V_{abs} does not correlate with the value of capacitance and in some cases voltages as large as 5 V to 8 V can be observed after a few hours for capacitors in the nanofarad range.
   d. The time to roll-off for V_{abs} and the rate of voltage decrease are related to the leakage currents in the capacitors. A simple model that is based on the Dow equivalent circuit for capacitors with absorption has been developed to explain long-term variations of absorption voltages and estimate insulation resistances in MLCCs.
   e. The suggested method that is based on monitoring long-term variations of V_{abs} allows for estimations of the insulation resistances up to 10^{14} Ω. Measurements of insulation resistance in MLCCs using a standard technique fail to reveal capacitors with cracks, whereas the voltage absorption technique was effective in more than 70% of cases

XIII. References

[1] G. G. Raju, *Dielectrics in electric fields*: CRC Press, Marcel Dekker, p. 592, 2003.

[2] B. Nagaraj, S. Aggarwal, and R. Ramesh, "Influence of contact electrodes on leakage characteristics in ferroelectric thin films," *Journal of Applied Physics*, vol. 90, pp. 375-382, Jul 2001.

[3] K. Hyyppa, "Dielectric Absorption in Memory Capacitors," *Instrumentation and Measurement, IEEE Transactions on*, vol. 21, pp. 53-56, 1972.
[4] B. Pease. (1982, October 13). Understand Capacitor Soakage to Optimize Analog Systems. *EDN*. Available: http://www.national.com/rap/Application/0,1570,28,00.html
[5] E. R. Neagu and R. M. Neagu, "Analysis of charging and discharging currents in polyethyleneterephtalate," *Physica Status Solidi a-Applied Research*, vol. 144, pp. 429-440, Aug 1994.
[6] R. Shaikh and G. R. G. Raju, "Electrical conduction in polyimide-FEP fluoropolymer films," in *Electrical Insulation and Dielectric Phenomena, 2002 Annual Report Conference on*, 2002, pp. 578-581.
[7] F. Smith, H. Neuhaus, S. Senturia, Z. Feit, D. Day, and T. Lewis, "Electrical conduction in polyimide between 20 and 350° C," *Journal of Electronic Materials*, vol. 16, pp. 93-106, 1987.
[8] F. C. Aris and T. J. Lewis, "Steady and Transient Conduction Processes in Anodic Tantalum Oxide," *Journal of Physics D-Applied Physics*, vol. 6, pp. 1067-1083, 1973.
[9] R. M. Fleming, D. V. Lang, and C. D. Jones, "Defect dominated charge transport in amorphous Ta2O5 thin films," *Journal of Applied Physics*, vol. 88, pp. 850-862, Jul 15 2000.
[10] A. Teverovsky, "Reverse bias behavior of surface mount tantalum capacitors," in *Capacitor and Resistor Technology Symposium, CARTS*, New Orleans, LA, 2002, pp. 105-123.
[11] X. Xu, M. Niskala, A. Gurav, M. Laps, and K. Saarinen, "Advances in Class-I C0G MLCC and SMD Film Capacitors," in *The 28th symposium for passive components, CARTS'07*, Newport Beach, CA, 2008.
[12] H. Bachhofer, H. Reisinger, H. Schroeder, T. Haneder, C. Dehm, H. Von Philipsborn, and R. Waser, "Relaxation effects and steady-state conduction in non-stoichiometric SBT films," *Integrated Ferroelectrics*, vol. 33, pp. 245-252, 2001.
[13] H. Y. Lee, K. C. Lee, J. N. Schunke, and L. C. Burton, "Leakage currents in multilayer ceramic capacitors," *IEEE Transactions on Components Hybrids and Manufacturing Technology*, vol. 7, pp. 443-453, 1984.
[14] H. Kliem, "Kohlrausch relaxations: new aspects about the everlasting story," *Dielectrics and Electrical Insulation, IEEE Transactions on*, vol. 12, pp. 709-718, 2005.
[15] M. Kuehn, B. Martin, and H. Kliem, "Computational investigations on the Kohlrausch empirical law in interacting systems," in *Electrical Insulation and Dielectric Phenomena, 2005. CEIDP '05. 2005 Annual Report Conference on*, 2005, pp. 373-376.
[16] J. C. Kuenen and G. C. M. Meijer, "Measurement of dielectric absorption of capacitors and analysis of its effects on VCOs," *Instrumentation and Measurement, IEEE Transactions on*, vol. 45, pp. 89-97, 1996.
[17] J. Burnham, S. L. Webster, W. J. Simmons, and J. W. Borough, "A Study of Dielectric Absorption in Capacitors by Thermally Stimulated Discharge (TSD) Tests," in *Reliability Physics Symposium, 1976. 14th Annual*, 1976, pp. 147-156.
[18] C. Iorga, "Compartmental analysis of dielectric absorption in capacitors," *Dielectrics and Electrical Insulation, IEEE Transactions on*, vol. 7, pp. 187-192, 2000.
[19] R. Anklekar, J. Fish, J. Christofferson, and V. Cooke, "Insulation Resistance Testing of High-Capacitance BME Multilayer Ceramic Capacitors," in *CARTS'03, the 23th Symposium for Passive Components*, Scottsdale AZ, 2003, pp. 86-95.
[20] A. Teverovsky, "Thermal Shock Testing and Fracturing of MLCCs under Manual Soldering Conditions," *IEEE Transactions on Device and Materials Reliability* vol. 12, pp. 413-419, 2012.
[21] P. C. Dow, "An Analysis of Certain Errors in Electronic Differential Analyzers II-Capacitor Dielectric Absorption," *Electronic Computers, IRE Transactions on*, vol. EC-7, pp. 17-22, 1958.
[22] S. Westerlund and L. Ekstam, "Capacitor theory," *Dielectrics and Electrical Insulation, IEEE Transactions on*, vol. 1, pp. 826-839, 1994.
[23] A. M. Holladay, "Unstable insulation resistance in ceramic capacitors " *Proceedings of Capacitor Technologies, Applications and Reliability, NASA*, pp. 27-31, 1981.
[24] M. Sampson, J. Brusse, and A. Teverovsky, "Humidity Steady State Low Voltage Testing of MLCCs (Based on NESC Technical Assessment Report)," in *CARTS USA*, Jacksonville, Fl, 2011.
[25] L. C. Burton, "Intrinsic mechanisms of multilayer ceramic capacitor failure," Virginia Polytechnic Inst. and State Univ., Blacksburg, VA, ADA199113, 1998.
[26] M. Dawber, K. M. Rabe, and J. F. Scott, "Physics of thin-film ferroelectric oxides," *Reviews of Modern Physics*, vol. 77, pp. 1083-1130, Oct 2005.
[27] J. H. Koh, B. M. Moon, and A. Grishin, "Dielectric properties and Schottky barriers in silver tantalate-niobate thin film capacitors," *Integrated Ferroelectrics*, vol. 39, pp. 1361-1368, 2001.
[28] L. Pintilie, I. Vrejoiu, D. Hesse, G. LeRhun, and M. Alexe, "Ferroelectric polarization-leakage current relation in high quality epitaxial Pb(Zr, Ti)O-3 films," *Physical Review B*, vol. 75, Mar 2007.
[29] J. C. Shin, J. Park, C. S. Hwang, and H. J. Kim, "Dielectric and electrical properties of sputter grown (Ba,Sr)TiO3 thin films," *JOURNAL OF APPLIED PHYSICS*, vol. 86, pp. 506-513, Jul 1999.
[30] E. Loh, "A model of dc leakage in ceramic capacitors," *Journal of Applied Physics*, vol. 53, pp. 6229-6235, 1982.

[31] P. Zubko, D. J. Jung, and J. F. Scott, "Electrical characterization of PbZr0.4Ti0.6O3 capacitors," *Journal of applied physics*, vol. 100, Dec 2006.
[32] F. D. Morrison, P. Zubko, D. J. Jung, J. F. Scott, P. Baxter, M. M. Saad, R. M. Bowman, and J. M. Gregg, "High-field conduction in barium titanate," *Applied Physics Letters*, vol. 86, Apr 2005.
[33] J. G. Simmons, "Richardson-Schottky effect in solids," *Physical Review Letters*, vol. 15, pp. 967-968, 1965.
[34] M. A. Lampert and P. Mark, *Current injection in solids*: Academic Press, p. 351, 1970.
[35] M. A. Lampert, A. Many, and P. Mark, "Space-Charge-Limited Currents Injected from a Point Contact," *Physical Review*, vol. 135, pp. A1444-A1453, 1964.
[36] L. C. Burton, "Voltage dependence of activation energy for multilayer ceramic capacitors," *Ieee Transactions on Components Hybrids and Manufacturing Technology*, vol. 8, pp. 517-524, Dec 1985.